HDAC3 Inhibition Promotes Antitumor Immunity by Enhancing CXCL10-Mediated Chemotaxis and Recruiting of Immune Cells

Lili Li[1,2], Shumin Hao[1,2], Meiling Gao[1,2], Junxiao Liu[1,2], Xin Xu[1,2], Jianfei Huang[3], Genhong Cheng[4], and Heng Yang[1,2,5]

ABSTRACT

It is generally believed that histone deacetylase (HDAC) inhibitors, which represent a new class of anticancer agents, exert their antitumor activity by directly causing cell-cycle arrest and apoptosis of tumor cells. However, in this study, we demonstrated that class I HDAC inhibitors, such as Entinostat and Panobinostat, effectively suppressed tumor growth in immunocompetent but not immunodeficient mice. Further studies with *Hdac1, 2*, or *3* knockout tumor cells indicated that tumor-specific inactivation of HDAC3 suppressed tumor growth by activating antitumor immunity. Specifically, we found that HDAC3 could directly bind to promotor regions and inhibit the expression of CXCL9, 10, and 11 chemokines. *Hdac3*-deficient tumor cells expressed high levels of these chemokines, which suppressed tumor growth in immunocompetent mice by recruiting $CXCR3^+$ T cells into the tumor microenvironment (TME). Furthermore, the inverse correlation between HDAC3 and CXCL10 expression in hepatocellular carcinoma tumor tissues also suggested HDAC3 might be involved in antitumor immune regulation and patient survival. Thus, our studies have illustrated that HDAC3 inhibition suppresses tumor growth by enhancing immune cell infiltration into the TME. This antitumor mechanism may be helpful in guiding HDAC3 inhibitor–based treatment.

Introduction

Histone deacetylases (HDAC) regulate target gene expression by removing acetyl groups from acetylated lysine residues of histone and nonhistone proteins. The HDAC superfamily comprises 18 members that are characterized into four classes: class I (HDACs1, 2, 3, and 8), class II (HDACs 4, 5, 6, 7, 9, and 10), class III (sirtuin family, sirt1-sirt7), and class IV (HDAC11; refs. 1, 2). Several studies have highlighted HDAC aberrant expression in certain cancer cells, and HDACs are considered as excellent targets for anticancer therapy (3–5). HDAC inhibitors, Vorinostat, Romidepsin, Panobinostat, and Belinostat, have been approved by the FDA for cancer therapy, and Tucidinostat also has been approved for clinical use in China. With scientific research and clinical trials continuously exploring new HDAC inhibitors that target specific HDAC proteins and are suitable for various cancers (3, 6, 7), more research on the detailed functions of individual HDAC proteins on carcinogenesis and the mechanisms involved is needed.

HDAC3 belongs to the class I HDACs, which were first identified as the components of the nuclear receptor corepressor (N-CoR) and silencing mediator of retinoic and thyroid receptors (SMRT) corepressor complexes (8). Aberrant expression and/or the location of HDAC3 correlates with carcinogenesis, and selective HDAC3 inhibitors have been developed (9–11). HDAC3 is involved in carcinogenesis by impacting cell-cycle progression or apoptosis of tumor cells, chromatin structure, and epigenetic modification or regulation of tumor-associated genes (12–16). Deletion or inhibition of HDAC3 leads to impaired DNA repair, reduced chromatin compaction and heterochromatin content, and delay cell-cycle progression (12, 13). As an epigenetic and transcriptional regulator, HDAC3 targets hyperacetylated H3K9 (H3K9ac)/trimethylation of H3K9 (H3K9me3) transition to regulate both DNA damage repair and transcription of many tumor-related genes in hepatocellular carcinoma (HCC; ref. 10). BCL6/SMRT/HDAC3 complexes mediate aberrant transcriptional silencing of genes that regulate B-cell signaling and immune response in CREBBP-mutated B-cell lymphoma, and selective inhibition of HDAC3 is reported to be a novel mechanism-based immune epigenetic therapy for CREBBP-mutant lymphomas (14, 15). HDAC3 directly regulates the expression of antitumor immunity-related genes, such as stimulator of interferon genes, PD-L1, and B7x (17–19). These studies shed light on the critical role and complex participation of HDAC3 in carcinogenesis and antitumor immunity.

HDAC3 affects different tumor types and cell lines, and the function of HDAC3 includes transcription regulation, metabolism regulation, or deacetylation modification. The involvement of HDAC3 in antitumor immunity has been extensively investigated, and the HDAC3-selective inhibitors are currently considered as a potential therapeutic strategy to combat various cancers (11, 20, 21). However, the impact of HDAC3 proteins on T-cell recruitment, especially in the context of CXCL9, 10, 11/CXCR3 chemotaxis into the tumor microenvironment (TME), has not been investigated sufficiently.

[1]Institute of Systems Medicine, Chinese Academy of Medical Sciences & Peking Union Medical College, Beijing, P.R. China. [2]Suzhou Institute of Systems Medicine, Suzhou, P.R. China. [3]Department of Clinical Biobank, Affiliated Hospital of Nantong University, Nantong, P.R. China. [4]Department of Microbiology, Immunology and Molecular Genetics, University of California, Los Angeles, Los Angeles. [5]National Key Laboratory of Medical Immunology, Shanghai, China.

L. Li, S. Hao, M. Gao, and J. Liu contributed equally to this article.

Corresponding Authors: Heng Yang, Institute of Systems Medicine, Chinese Academy of Medical Sciences & Peking Union Medical College, Beijing 100005, China. Phone: 86-512-62871526; Fax: 86-512-62873779; E-mail: yhmyt@hotmail.com; Genhong Cheng, gcheng@mednet.ucla.edu; and Jianfei Huang, jfhuang@ntu.edu.cn

Cancer Immunol Res 2023;11:657–73

doi: 10.1158/2326-6066.CIR-22-0317

Infiltration of immune cells into the TME is controlled by chemokines, which are small proteins that induce chemotaxis, promote differentiation of immune cells, and cause tissue extravasation. They play an important role in antitumor immune responses in the TME (22–24). The CXCL9, 10, 11/CXCR3 axis can lead to tumor suppression by regulating immune cell migration, differentiation, and activation (25–27). CXCL9, 10, 11 are mainly secreted by monocytes, endothelial cells, fibroblasts, and cancer cells in response to IFNγ and IFNβ (28, 29). These chemokines are selective ligands for CXCR3, which is preferentially expressed on the surface of monocytes, T cells, natural killer cells, dendritic cells (DC), and cancer cells (30). The CXCL9, 10, 11/CXCR3 axis is involved in antitumor responses and promotes metastasis through paracrine and autocrine axes. The CXCL9, 10, 11/CXCR3 axis activates antitumor immune responses by regulating immune cell migration, differentiation, and activation (paracrine axis) (25). Zhang and colleagues report that the combination of plasmid-borne CXCL9 plus cisplatin augments colon and lung cancer reduction and CTL activation (31). Intratumoral CXCL9 and systemic IL2 reduces tumor growth and angiogenesis in a renal cell carcinoma tumor model through tumor-infiltrating $CXCR3^+$ mononuclear cells. The benefit of CXCL10 overexpression to inhibit tumor growth has been reported in melanoma, sarcoma, and lung carcinoma models (25). Although activation of the CXCL9, 10, 11/CXCR3 axis is a promising approach for cancer treatment, some reports show that suppression of this axis decreases tumor metastasis (autocrine axis), and treatment with the CXCR3 antagonist AMG487 inhibits colorectal cancer and osteosarcoma lung metastases (32, 33). These findings indicate the complex involvement of the CXCL9, 10, 11/CXCR3 axis in antitumor immunity.

In this work, we found that HDAC inhibitors effectively suppressed tumor growth in C57BL/6 mice but not in nude mice. We also found that *Hdac3*$^{-/-}$ tumors grew at much slower rates than *Hdac3*$^{+/+}$ tumors in C57BL/6 mice, although they grew at similar rates in nude mice. These data demonstrated a novel role of HDAC3 in regulating the TME and antitumor immunity. Our mechanistic research revealed that HDAC3 suppressed *Cxcl9, 10, 11* expression by directly binding to and deacetylating proteins near their promotor regions. Taking advantage of tissue microarray-IHC (TMA-IHC), we found that HDAC3 expression in HCC tissues showed a modest but significant inverse correlation with CXCL10 expression, $CD8^+$ T-cell infiltration, and patient survival, indicating the possible regulatory relationship between HDAC3 and CXCL10 in the human TME. Thus, our work not only highlights the value of HDAC3 inhibition in cancer treatment, but also provides a novel TME regulating mechanism mediated by HDAC3.

Materials and Methods

Cell lines, antibodies, and reagents

The MCA205 fibrosarcoma cell line was generated and provided by Dr. S. A. Rosenberg (NCI, Bethesda, MD) in 2015. MC38 murine colon adenocarcinoma and human embryonic kidney 293T cell lines were purchased from Cell Resource Center, Institute of Basic Medical Sciences, Chinese Academy of Medical Sciences (Beijing, P.R. China) in 2019. Authentication of tumor cell lines (MCA205, MC38, 293T) with short tandem repeat DNA profiles was performed every year with Procell Life Science & Technology Co., Ltd. *Mycoplasma* contamination was tested by PCR with cell culture supernatants (Beyotime, catalog no. C0301S). Normocin (InvivoGen, catalog no. ant-nr-1) and plasmocure (InvivoGen, catalog no. ant-pc) were used to clean the contamination when *Mycoplasma* was detected. Only cell lines free of *Mycoplasma* were used in this study. MCA205 and MC38 cells were cultured in DMEM (Thermo Fisher Scientific, catalog no. 11995040) supplemented with 10% FBS (Thermo Fisher Scientific, catalog no. 10099141), 100 U/mL penicillin, and 50 μg/mL streptomycin (Thermo Fisher Scientific, catalog no. 15140122). For subculturing MCA205, MC38, and 293T cells: the spent culture medium was removed, and the attached cells were washed using PBS (Gibco, catalog no. C1001050013T) and incubated with prewarmed trypsin (Gibco, catalog no. 25200-072) at room temperature for approximately 2 minutes. The prewarmed culture medium was added to neutralize trypsin activity, and the cells were transferred to a 15 mL conical tube, centrifuged at 1,000 rpm for 3 minutes, resuspended with culture medium, and the cell density was counted. The cell suspension was then diluted to seeding density and the appropriate volume was added into new cell culture vessels. All cells were incubated at 37°C in a humidified air atmosphere with 5% CO_2. Cells were plated at 2×10^5 cells/well in 6-well plate for overexpression and deletion experiments and at 8×10^5 cells/well for Western blot analysis and qRT-PCR experiments. Cells underwent about four passages in culture before experiments. The cell harvesting was similar to the culture method after resuspending the pellet with PBS, centrifugation and discarding the PBS, and adding corresponding lysis reagents.

Hdac1$^{-/-}$, *Hdac2*$^{-/-}$, *Hdac3*$^{+/-}$, *Hdac3*$^{-/-}$ and overexpression cell line generation

To generate *Hdac1*$^{-/-}$, *Hdac2*$^{-/-}$, *Hdac3*$^{+/-}$ and *Hdac3*$^{-/-}$ MCA205 and MC38 cell lines, single-guide RNA (sgRNA) sequences targeting *Hdac1, 2, 3* were selected from a sgRNA library (a gift from Dr. Feng Zhang), synthesized (by GENEWIZ in Suzhou), and cloned into the lentiCRISPR V2 vector (a gift from FengZhang, Addgene_52961). Lentivirus was produced in 293T cells by cotransfection of pMD2.G (Addgene_12259), psPAX2 (Addgene_12260) and sgRNA plasmids or control vector plasmid. Virus supernatant was collected 48 hours after transfection and filtered with a 0.45 μmol/L filter. MCA205 or MC38 cells were infected with above viruses. After a 48-hour transfection, cells were cultured in puromycin (4 μg/mL; InvivoGen, catalog no. ant-pr-1) selection medium for 7 days. Monoclonal cells cultured in 96-well plate were acquired by FACS Aria III cell sorter (BD). Gene knockdown or knockout cells were selected and verified by Western blot assay using the corresponding antibody. The sequences of the sgRNAs used in this study were listed in Supplementary Fig. S1.

To generate wild-type (WT) and H134/135Q-mutant HDAC3-overexpressing cells, WT and H134/135Q-mutant HDAC3 coding sequences were cloned and inserted into VP64-GFP (Addgene_70228) vector by standard molecular procedure. Lentiviruses were produced in 293T cells by cotransfection of pMD2.G (Addgene_12259), psPAX2 (Addgene_12260), and VP64-GFP plasmids overexpressing WT or H134/135Q-mutant HDAC3 or vector control. Virus supernatant was collected 48 hours after transfection, *Hdac3*$^{-/-}$ cells were infected with above viruses for 48 hours, then GFP^+ cells were enriched by FACS Aria III cell sorter (BD). Ovalbumin (OVA)-expressing WT and *Hdac3*$^{+/-}$ MCA205 cells (OVA-MCA205 and OVA-*Hdac3*$^{+/-}$ MCA205) were established by transfection with pCI-neo-mOVA plasmid (Addgene_25099) and selected with G418 (Thermo Fisher Scientific, catalog no. 10131035). The gene overexpressing cell lines were verified by Western blot analysis.

In vitro tumor cell treatment and assays

WT and *Hdac3*$^{-/-}$ MCA205 cells were seeded in 6-well plate and cultured overnight. For IFN treatment assays, cells were treated with

100 U/mL IFNα (Pblassay science, catalog no. 12105-1), 10 ng/mL IFNβ (R&D, catalog no. 8234-MB-010/CF), 100 U/mL IFNγ (R&D, catalog no. 485-MI-100/CF), or vehicle control (0.1% BSA, MCE, catalog no. HY-D0842) for 6 hours. The culture supernatant was then collected for ELISAs, and cells were lysed with TRIzol (Thermo Fisher Scientific, catalog no. 15596026) for qRT-PCR. For HDAC inhibitor treatment, cells were treated with 2.5 μmol/L RGF966 (Selleck, catalog no. S7229), 10 μmol/L Entinostat (Selleck, catalog no. S1053), or DMSO control for 6 hours. A total of 100 U/mL IFNα, 10 ng/mL IFNβ, 100 U/mL IFNγ, or vehicle control were then added to the cells. A total of 6 hours after IFN treatment, cells were lysed with TRIzol for qRT-PCR. For methotrexate (MTX) treatment, WT or *Hdac3*$^{-/-}$ MCA205 cells were treated with 2 μmol/L MTX (MCE, catalog no. HY-14519) for 3 hours. The cells were then counted and inoculated into mice at 1×10^6 cell/mouse. For chromatin immunoprecipitation sequencing (ChIP-seq) and ChIP-qPCR, WT, *Hdac3*$^{+/-}$, *Hdac3*$^{-/-}$ MCA205 cells and *Hdac3*$^{-/-}$ MCA205 overexpressing WT, H134/135Q-mutant HDAC3, or vector control cells were seeded in a 15 cm dish at the density of 1×10^7 cells/dish and cultured overnight. Then the cells were treated with PBS vehicle or 10 ng/mL IFNβ for 3 hours until ChIP assay.

Cell proliferation and viability analyses

Cell proliferation of WT and *Hdac3*$^{-/-}$ MCA205 and MC38 cells was analyzed with a Cell Counting Kit-8 (Beyotime, catalog no. C0038) according to supplier's recommendations. The expression of Ki67 in WT and *Hdac3*$^{-/-}$ MCA205 and MC38 cells was determined via staining with FITC-Ki67 (BioLegend, catalog no. 151211) or FITC-rat IgG isotype (BioLegend, catalog no. 401913) using a standard flow cytometry staining protocol. The samples were acquired with Attune NxT Flow Cytometer (Thermo Fisher Scientific) and analyzed with FlowJo software (Tree Star, Inc.). For single clone formation assays, WT and *Hdac3*$^{-/-}$ MCA205 and MC38 cells were seeded in 6-well plate at the density of 200 cells/well. Seven days after culture, the plates were stained with crystal violet staining solution (Solarbio, catalog no. G1062), and the clones were counted.

Mouse experiments

The animal study was reviewed and approved by The Ethics Committee of Suzhou Institute of Systems Medicine (ISM-IACUC-0107-R). Female C57BL/6 and nude mice ages between 6 and 8 weeks were purchased from Beijing Vital River Laboratory Animal Technology Co. Ltd. All animals were bred in our core animal facility. Age- and sex-matched mice were randomly assigned to different groups in the same experiment with the following strategy. A total of 2×10^6/mouse MC38 or 1×10^6/mouse MCA205 cells were subcutaneously inoculated in C57BL/6 or nude mice. Seven days after inoculation, mice were treated with Entinostat (30 mg/kg, intragastrically), Panobinostat (Selleck, catalog no. S1030, 20 mg/kg, intraperitoneally), or vehicle control (DMSO, Solarbio, catalog no. D8371, intragastrically for Entinostat control and intraperitoneally for Panobinostat control) three times per week, and tumor growth was monitored.

For tumor growth comparisons, 2×10^6/mouse MC38 (WT, *Hdac1*$^{-/-}$, *Hdac2*$^{-/-}$, *Hdac3*$^{-/-}$, *Hdac3*$^{+/-}$) or 1×10^6/mouse MCA205 (WT, *Hdac3*$^{+/-}$, *Hdac3*$^{-/-}$ cell lines and *Hdac3*$^{-/-}$ cell lines overexpressed with WT, H134/135Q-mutant HDAC3 or vector control) cells were subcutaneously inoculated in C57BL/6 or nude mice for 28 days and tumor growth was monitored. For survival experiments, 1×10^6 WT and *Hdac3*$^{+/-}$ MCA205 cells were inoculated in C57BL/6 mice by intravenous injection, and the overall survival (OS) ratio of mice were monitored.

In addition, 1×10^6/mouse WT and *Hdac3*$^{+/-}$ MCA205 cells were inoculated in C57BL/6 mice. Mice with xenograft *Hdac3*$^{+/-}$ MCA205 tumors were treated intravenously with anti-CXCR3 antibody (BioXcell, catalog no. BE0249), anti-TNFα (BioXcell, catalog no. BE0058), or IgG control (BioXcell, catalog no. BE0091) at 7, 9, and 11 days after tumor inoculation (10 mg/kg), and tumor growth was monitored.

Moreover, 1×10^6/mouse WT MCA205 cells were inoculated in the left side of C57BL/6 mice. Seven days after inoculation, PBS (Gibco, catalog no. 10010023) control or 1×10^6/mouse MTX-treated (2 μmol/L, 3 hours) WT, *Hdac3*$^{+/-}$or *Hdac3*$^{-/-}$ MCA205 cells were inoculated in the right side of mice. Tumor growth in the left side was monitored. For anti-CXCR3 antibody treatment: after the MTX-treated cells were inoculated, IgG control or anti-CXCR3 (10 mg/kg) was intravenously administrated at 1, 3, 5 days after inoculation. Tumor growth in the left side was monitored.

For all mouse experiments, the measurement or quantification of primary tumor samples, investigators were blinded to group assignments. Tumor growth was monitored two to three times per week with an electronic caliper. Animals were sacrificed when the volume of tumors reached 300 mm^2. All mice were sacrificed by asphyxiation CO_2.

Tissue dissociation

WT, *Hdac3*$^{+/-}$ or *Hdac3*$^{-/-}$ MCA205 tumors were stripped with surgical scissors and blade on day 7 postimplantation for flow cytometry analysis, immunofluorescence staining, enzyme-linked immune spot (ELISpot) assay, ELISA, and RNA sequencing (RNA-seq). For flow cytometry analysis and ELISpot assays, freshly recovered WT and *Hdac3*$^{+/-}$ MCA205 tumors were cut into small pieces with surgical scissors in digestion buffer: serum-free RPMI1640 medium (Gibco, catalog no. 11875119) containing 0.4 Wnsch units/mL Liberase TL (Roche, catalog no. 05401020001), and 200 U/mL DNase I (Calbiochem, catalog no. 260913-10MUCN). The tumor tissues were incubated at 37°C for 30 minutes, and the cell suspension was filtered through 70 μm cell strainers. The prepared single-cell suspensions were then used for analysis. For immunofluorescence staining, freshly collected WT and *Hdac3*$^{+/-}$ MCA205 tumors were treated with 4% paraformaldehyde (PFA; Beyotime, catalog no. P0099) at room temperature for 4 hours. PFA-fixed tumors were transferred into 30% (wt/vol) sucrose solution for 24 hours. The tumors were embedded in optimum cutting temperature compound (Solarbio, catalog no. 4583) and then frozen at −80°C. Frozen tissue sections were obtained with CM1950 Cryostats (Leica Biosystems) and stored at −80°C. For ELISAs and RNA-seq, WT and *Hdac3*$^{+/-}$ MCA205 tumors were dissociated by liquid nitrogen grounding and lysed with TRIzol (Thermo Fisher Scientific, catalog no. 15596026) for RNA-seq and PBS supplemented with protease inhibitors (Roche, catalog no. 12352200) for ELISAs.

Immunofluorescence staining

Frozen tissue sections were recovered to room temperature, fixed with 2% PFA for 15 minutes, and permeabilized with 0.5% Triton-X100 (Sigma, catalog no. T8787) for 5 minutes. Tissue sections were then blocked with 20% FBS for 20 minutes and stained with anti-mouse primary antibodies [CD4 (catalog no. ab133616), CD8 (catalog no. ab217344), and IFNγ (clone XMG1.2; catalog no. ab23637) from Abcam, dilution at 1:100] at room temperature for 2 hours. After washing three times with 1× PBST (Solarbio, catalog no. P1033), the tissue sections were stained with fluorescent dye–conjugated

secondary antibodies [Goat anti-rabbit IgG conjugated with Alexa Fluor 568 (for CD4 and CD8, Thermo Fisher scientific, catalog no. A-11011), goat anti-rat IgG conjugated with FITC (for IFNγ, Thermo Fisher scientific, catalog no. 31584), dilution at 1:1,000] at room temperature for 1 hour. The tissue sections were then washed three times, followed by nuclear counterstaining with 4, 6-Amidine-2-phenylindoles (BBI Life Sciences, 1:1,000). After washing another three times, slides were sealed with Fluoromount-G mounting medium (Southern Biotech). Images were captured with a confocal microscope (Leica TCS SP8).

ELISA

The concentration of mouse CXCL9, 10, 11 cytokines was measured with ELISA kits (R&D, catalog nos. MCX900, DY466, and DY572) according to the manufacturer's instructions. Briefly, plates were coated with 100 μL/well diluted capture antibodies and incubated at 4°C overnight. After washing with 1× PBST for three times, the plates were blocked with 200 μL/well blocking buffer (1% BSA in PBS) and incubated at room temperature for 1 hour. After three washes, 100 μL/well diluted cell culture supernatants or tumor tissue lysis supernatants (1×, 2×, and 4× dilution with PBS) were added into the plates, followed by a 2-hour incubation at room temperature. After three washes, 100 μL/well diluted detection antibody was added into the plates, followed by room temperature incubation for 2 hours, and 100 μL/well diluted horseradish peroxidase (HRP)–Streptavidin was added into the plates, followed by room temperature incubation for 15 to 20 minutes. After three washes, 50 μL/well stop solution (2N H_2SO_4) was added into the plates, and the plates were read at 450 nm by SpectraMax i3 (Molecular Devices) plate reader. The concentrations of cytokines were calculated on the basis of the standard curve (with the kit).

ELISpot

The frequencies of IFNγ-secreting T cells in WT and *Hdac3*$^{+/-}$ MCA205 tumors (7 days after inoculation) were quantified with ELISpot assay kits from BD Biosciences (catalog no. 551881). OVA-MCA205 and OVA-*Hdac3*$^{+/-}$ MCA205 tumor tissues were enzymatically digested to single-cell suspensions as indicated above and resuspended in DMEM containing 10% FBS. For each sample, 1×10^6 cells were seeded per microwell in ELISpot plates precoated with anti-IFNγ capture antibody (BD Biosciences, catalog no. 51-2525KZ). After 16 hours of culture at 37°C in a 5% CO_2 and humidified incubator, the plates were washed with 1×PBST and incubated with biotinylated detection antibody (BD Biosciences, catalog no. 51-1818KA) for 1 hour. After washing and drying, the plates were inspected by CTL ImmunoSpot S6 Analyzers (CTL and CTL Analyzers, LLC) and spot counts were recorded.

Bulk RNA-seq on tumor-infiltrating CD4$^+$ and CD8$^+$ T cells and analysis

Tumor single-cell suspensions were prepared from 6 mice inoculated with WT ($n = 3$) or *Hdac3*$^{+/-}$ ($n = 3$) MCA205 cells for 6 days as described above. Dead cells were removed with vivid yellow staining (Invitrogen, catalog no. L34960). Cells were then stained with FITC anti-CD45 (30-F11; BioLegend, catalog no. 103107), PE anti-CD8a (53-7.6; BioLegend, catalog no. 100707), and APC-Cy7 anti-CD4 (GK1.5; BioLegend, catalog no. 100413) for 30 minutes. Sorting via FACS was performed on a FACS Aria III (BD Biosciences), and 1,000 CD45$^+$CD4$^+$ or CD45$^+$CD8$^+$ T cells from every tumor were sorted into separate tubes and resuspended in RNAlater (Thermo Fisher scientific, catalog no. AM7020). Full-length cDNA synthesis and amplification were prepared using SMART-Seq V4 Ultral Low Input RNA Kit (Takara, catalog no. R400752) for sequencing, which is based on the SMART-seq2 method (34). The Nextera XT DNA Library Preparation Kit (Illumina Inc., catalog no. 15032354) was then used to make cDNA libraries suitable for Illumina sequencing. Briefly, cDNA was fragmented, and an adapter was added using transposase, followed by limited-cycle PCR to enrich and add index to the cDNA fragments. The final library quality was assessed with an Agilent TapeStation. These libraries were sequenced using the Novaseq 6000 system (Illumina Inc.) with 2*150 bp paired-end sequencing.

Tumor RNA-seq and analysis

Total RNA from WT or *Hdac3*$^{+/-}$ MCA205 tumors ($n = 3$/group) was extracted using TRIzol reagent according to the manufacturer's instructions. The concentration and quality of RNA were measured by Agilent 2100 (Agilent Technologies) and an RNA LabChIP 6000 Nano kit [Agilent Technologies, catalog no. 5067-1511; RNA integrity numbers (RIN) of RNA samples used in this study were 7–10]. Next-generation sequencing (GENEWIZ) was performed after RNA-seq libraries were prepared with NEBNext Ultra II Direcrional RNA library Prep Kit (NEB, catalog no. E7760L) according to the manufacturer's instructions. Final library size distribution was 320 bp and sequenced on an Illumina Novaseq 6000 (Hiseq-PE150 sequencing strategy and paired end 2*150 bp reads length).

Bulk RNA-seq and RNA-seq data analysis

Raw sequencing data were filtered with CLC Genomics Workbench 12 (QIAGEN Bioinformatics) to remove low-quality and adapter bases. In CLC Trim tool, quality scores limit was 0.05 and maximum number of ambiguous nucleotides was 2. For sequencing alignment, filtered reads were mapped to *Mus_musculus*_en-sembl_80_sequence and GEVE reference sequences (http://geve.med.u-tokai.ac.jp/annotation-datasheet/) on CLC. Differential gene expression was determined using DESeq2, and genes were ranked according to the formation metric = −log(p,10)/log(FC,2) for gene set enrichment analysis (GSEA). We used the GSEA Preranked tool for GSEA and R studio software (R Foundation for Statistical Computing) for heat map and clusterProfiler analysis.

qRT-PCR

Total RNA from cultured IFN (α, β, γ) or HDAC inhibitors (RGF966 and Entinostat) treated WT and *Hdac3*$^{-/-}$ MCA205 cells and WT and *Hdac3*$^{+/-}$ tumor tissues from IgG and anti-CXCR3 antibody administrated mice were extracted using TRIzol reagent according to the manufacturer's instructions. RNA reverse transcription and cDNA were obtained with PrimeScript RT Reagent Kit (Takara, catalog no. RR037A). Gene expression assays were performed with SYRB master mix (Takara, catalog no. RR420A) with 200 ng cDNA as template in 20 μL reaction system in 96-well plate by LightCycler480 II (Roche). All experiments were repeated at least three times. Fold changes were calculated using the $\Delta\Delta C_t$ method and *Gapdh* was set as normalizing gene. qRT-PCR primers for mouse *Cxcl9, 10, 11, Cxcr3*, and *Gapdh* genes were obtained from PrimerBank (https://pga.mgh.harvard.edu/primerbank/), and the sequences of primers were as following:

Cxcl9-F: GGAGTTCGAGGAACCCTAGTG
Cxcl9-R: GGGATTTGTAGTGGATCGTGC
Cxcl10-F: CCAAGTGCTGCCGTCATTTTC
Cxcl10-R: GGCTCGCAGGGATGATTTCAA
Cxcl11-F: GGCTTCCTTATGTTCAAACAGGG
Cxcl11-R: GCCGTTACTCGGGTAAATTACA

Cxcr3-F: TACCTTGAGGTTAGTGAACGTCA
Cxcr3-R: CGCTCTCGTTTTCCCCATAATC
Gapdh-F: TGGATTTGGACGCATTGGTC
Gapdh-R: TTTGCACTGGTACGTGTTGAT

ChIP-seq and ChIP-qPCR assay

ChIP assays were performed using SimpleChIP Plus Enzymatic Chromatin IP Kit (Cell Signaling Technology, catalog no. 9005) according to the manufacturer's recommendations. Rabbit anti-HDAC3 (Cell Signaling Technology, catalog no. 85057), rabbit anti-H3K27ac (Cell Signaling Technology, catalog no. 8173), and Rabbit IgG antibodies (Cell Signaling Technology, catalog no. 3900; all antibodies were diluted at 1:40) were used to pull down the binding DNA sequences (4°C, overnight). Immunoprecipitated DNA sequences were purified and eluted for ChIP-seq (GENEWIZ) or ChIP-qPCR assay. For ChIP-seq, libraries were prepared using KAPA HyperPlus Kit (KAPA Biosystems, catalog no. KK8514) according to manufacturer's protocol. The libraries were then sequenced by 2*150 bp paired-end sequencing on the Novaseq system (Illumina Inc.). Data analysis was performed with CLC Genomics Workbench 12 according to the ChIP-seq analysis manuals (https://resources.qiagenbioinformatics.com/manuals/clcgenomicsworkbench/750/index.php?manual=ChIP_Seq_Analysis.html). For ChIP-qPCR, immunoprecipitated DNA samples were used as templates (2 μL in a 20 μL reaction system) and quantitative PCR was performed. Primers used for *Cxcl10* gene promotor detection were forward: 5′-TCTGCAAAGAGTTTCCCTCCC-3′, reverse: 5′-ACAAGCAATGCCCTCGGTT-3′. Rabbit IgG group was used as control for data normalization. Fold changes were calculated using the $\Delta\Delta C_t$ method.

Flow cytometry

Single-cell suspensions were incubated with a CD16/32 (clone 2.4G2) antibody (BioLegend, catalog no. 101301, 1:200) to block nonspecific staining on ice for 15 minutes, and the LIVE/DEAD Fixable Yellow Dead Cell Stain Kit (Thermo Fisher Scientific, catalog no. L34960) was used to exclude dead cells for further analyses. Then surface staining was performed with 2 μg/mL of the following fluorochrome-conjugated antibodies at 4°C for 30 minutes: PerCP/Cy5.5 anti-CD45 (30-F11, catalog no. 103131), PE/Cy7 anti-CD11c (N418, catalog no. 117317), FITC anti-CD8a (53-7.6, catalog no. 100705), APC/Cy7 anti-CD4 (GK1.5, catalog no. 100413), PerCP/Cy5.5 anti-CD11b (M1/70, catalog no. 101227), APC anti-F4/80 (BM8, catalog no. 123115), and APC anti-CXCR3 (CXCR3-173, catalog no. 126511) from BioLegend. For detecting IFNγ$^+$ cells, phorbol 12-myristate 13-acetate (Beyotime, catalog no. S1819) and Ionomycin (Beyotime, catalog no. S1672) were used to stimulated cells. After stimulation, cells were fixed and permeabilizated with fixation and permeabilization solutions kit (BD, catalog no. 554714), and stained with PE/Cy7 anti-IFNγ (XMG1.2, catalog no. 505825) at 4°C for 30 minutes. All the samples were acquired with Attune NxT Flow Cytometer (Thermo Fisher Scientific) and analyzed with FlowJo software (Tree Star, Inc.).

Western blot analysis

WT, *Hda3*$^{+/-}$, *Hdac3*$^{-/-}$ MCA205 and MC38 cells, *Hdac1*$^{-/-}$, *Hdac2*$^{-/-}$ MC38 cells, *Hdac3*$^{-/-}$ MCA205 overexpressing WT, H134/135Q-mutant HDAC3 or vector control and tumor samples from *Hdac3*$^{-/-}$ MCA205 overexpressing WT, H134/135Q-mutant HDAC3 or vector were lyzed with lysis buffer (Beyotime, catalog no. P0013C). The cell extracts (20 μg total protein/well) were immunoblotted [10% PAGE gel (Vazyme, catalog no. E303-01)] with the indicated antibodies to measure the level of the expressed proteins. Primary antibodies including mouse anti-β-actin (Cell Signaling Technology, catalog no. 3700), rabbit anti-HDAC1 (Cell Signaling Technology, catalog no. 34589), rabbit anti-HDAC2 (Cell Signaling Technology, catalog no. 57156), and rabbit anti-HDAC3 (Cell Signaling Technology, catalog no. 85057) antibodies were used for detection at the dilution of 1:1,000. Then HRP-conjugated anti-mouse (Cell Signaling Technology, catalog no. 7046) and anti-rabbit (Cell Signaling Technology, catalog no. 7074) secondary antibodies were used at the dilution of 1:5,000 and the membranes were scanned with ChemiDoc XRS+system (Bio-Rad).

Tumor tissues and clinical data

Clinical sample collection and usage were approved by the Ethical Committee of the Human Research Ethics Committee of the Affiliated Hospital of Nantong University (Nantong, P.R. China) and written informed consent from the patients was obtained. This study recruited 129 human patients with HCC at the Affiliated Hospital of Nantong University (Nantong, P.R. China), including malignant HCC samples ($n = 43$) and benignant HCC samples ($n = 86$). Tumor tissues were collected from patients with surgical tumor excision, fixed with formalin (Sigma, catalog no. 104003), embedded with paraffin (Solarbio, catalog no. YA0012), stored at room temperature, and then examined by at least two independent pathologists. All the patients had not received chemotherapy, radiotherapy, or immunotherapy before their surgeries. The clinical information of all patients was collected in detail, including age, sex, Hepatitis B virus (HBV) infection, liver cirrhosis, vascular invasion, tumor size, tumor differentiation, and tumor–node–metastasis stage. The study was conducted according to the principles of the Declaration of Helsinki and approved by the Ethical Committee of the Human Research Ethics Committee of the Affiliated Hospital of Nantong University (Nantong, P.R. China).

IHC measurement and analysis of TMA

TMA-IHC was performed to measure the expression of HDAC3, CD8a, CXCL10, and CXCR3 in tissue blocks. The core tissue biopsies (2 mm in diameter) taken from individual paraffin-embedded sections were rearrayed in recipient paraffin blocks by using a TMA system (Quick-Ray, UT06, UNITMA; ref. 35). Sections from arrayed blocks were sliced into 4 μm and stained with a monoclonal rabbit anti-human HDAC3 (Cell Signaling Technology, catalog no. 85057), anti-human CD8 (Abcam, catalog no. ab199016), anti-human CXCR3 (Invitrogen, catalog no. PA5-23104), and anti-human CXCL10 (Abcam, catalog no. ab8098; all antibodies used at the dilution of 1:100) at 4°C overnight, followed by incubation with a biotinylated secondary antibody (Abcam, catalog no. 64256) at room temperature for 30 minutes. HDAC3, CD8a, CXCL10, and CXCR3 scores were calculated with the percentage of fluorescence-positive cells/CK staining cells×100 (0%–100%). The Vectra 3.0 Automated Quantitative Pathology Imaging System (PerkinElmer company) was used to accurately calculate cell counts of different HDAC3, CD8, CXCR3, and CXCL10 staining intensities in specific tissues. The expression of HDAC3 protein was graded by one two-grade scoring system, and we chose 50% as the cut-off point: a score of 0% to 50% was regarded as no or low expression, whereas 50% to 100% was regarded as high expression.

Dataset analysis for OS

To verify the prognostic value of *Hdac1, 2, 3* genes, human datasets from a total of 876 patients with gastric cancer were obtained from The Cancer Genome Atlas (TCGA) database (https://www.cancer.gov/

about-nci/organization/ccg/research/structural-genomics/tcga). The entire database incorporates 876 gastric cancer samples, gene expression data [published in Gene Expression Omnibus (GEO) as GSE22377, GSE14210, and GSE51105]. These patients were divided into different groups according to the expression of *Hdac1, 2, 3* genes, with the best performing threshold to separate the low and high quartiles as the cutoff. OS rates were analyzed with a Kaplan–Meier plotter (https://kmplot.com/analysis/). The HR with 95% confidence intervals and log-rank *P* value were calculated with GraphPad Prism 8.0 software (GraphPad Software).

Statistical analysis

In mouse experiments, mice with the same age and sex were randomly assigned to different groups in the same experiment. Statistical analyses were performed with GraphPad Prism 8 software and R Studio version 3.6.3. All results are presented as means ± SD. Tumor progression curves were compared by calculating the AUC of individual mice, and statistics were done with a two-tailed Mann–Whitney *U* test. The strength of association between two variables and the direction of the relationship were explored with nonparametric correction coefficient analysis (Spearman), and the one-tailed *P* value was calculated. In qRT-PCR, ChIP-PCR, ELISA, and FACS experiments, all results are presented as means ± SD. For the human HCC TMA-IHC, scatter plots are shown as means ± SEM. Statistical differences were analyzed by one-way ANOVA or unpaired two-tailed Student *t* tests. *P* values were indicated by ns, not significant; *, $P < 0.05$; **, $P < 0.01$; ***, $P < 0.001$; and ****, $P < 0.0001$.

Data availability

Raw data for tumor RNA-seq, ChIP-seq, and bulk RNA-seq are deposited at the NCBI BioProject database (accession nos.: PRJNA893757 and PRJNA893856). Further information and requests for resources and regents should be directed to the corresponding authors. All requests for raw data, analyzed data, and materials will be promptly reviewed by the corresponding author to verify whether the request is subject to any intellectual property or confidentially obligations. Any data and materials that can be shared will be released via a Materials Transfer Agreement.

Results

HDAC inhibitors suppress tumor growth in an immune-dependent manner

HDAC inhibitors have been extensively explored for cancer therapy. Among them, Panobinostat (also known as LBH589, a pan HDAC inhibitor) and Entinostat (also known as MS275, HDAC1 and 3 selective inhibitor) are under phase III clinical trials. We first checked the effect of Entinostat and Panobinostat on the growth of MC38 murine colon adenocarcinoma and MCA205 fibrosarcoma tumors. We found that Entinostat and Panobinostat effectively suppressed the growth of MC38 and MCA205 tumors in immunocompetent C57BL/6 mice (**Fig. 1A–D**), but not in immunodeficient nude mice (**Fig. 1E–H**). These results indicate that the class I HDAC inhibitors Entinostat and Panobinostat inhibit MCA205 and MC38 tumor growth in an immune-dependent manner.

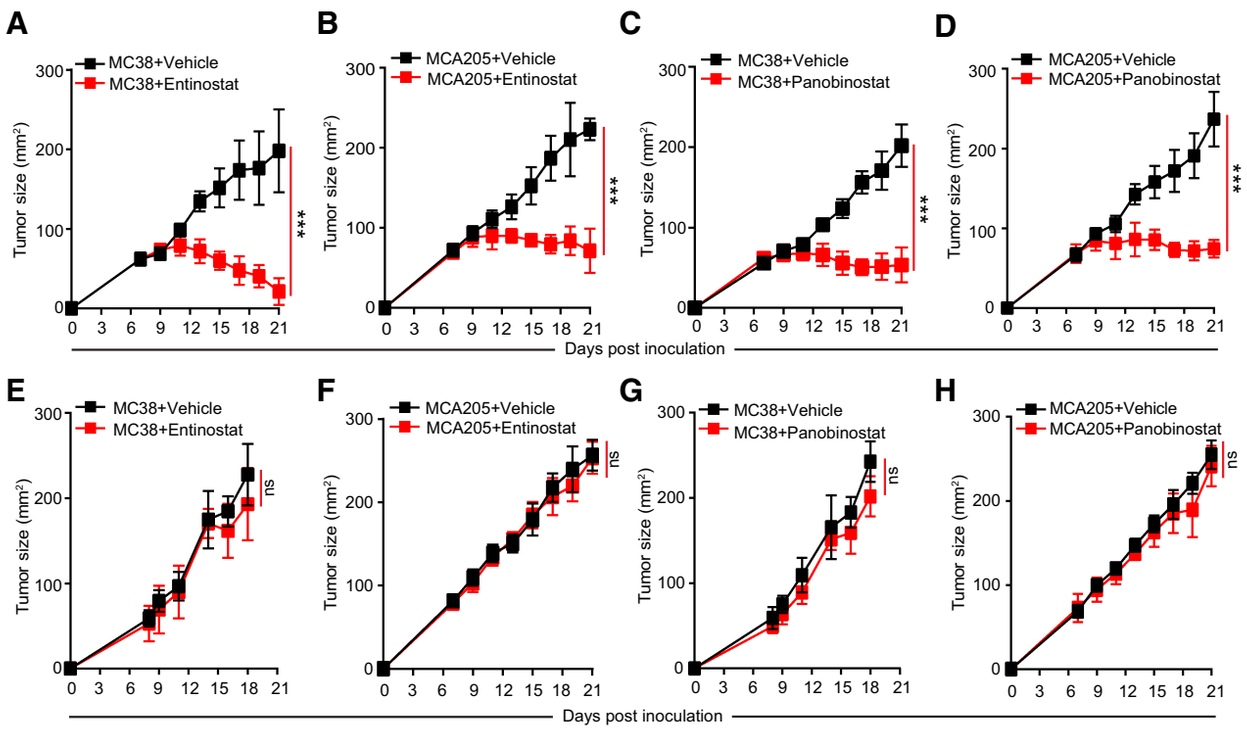

Figure 1.

HDAC inhibitors suppress tumor growth in an immune-dependent manner. MC38 (**A**, **C**, **E**, and **G**) and MCA205 cells (**B**, **D**, **F**, and **H**) were inoculated in C57BL/6 (**A–D**) or nude mice (**E–H**) subcutaneously. Seven days after inoculation, tumor-bearing mice were treated with HDAC inhibitors Entinostat (30 mg/kg, intragastrically; **A**, **B**, **E**, and **F**), Panobinostat (20 mg/kg, intraperitoneally; **C**, **D**, **G**, **H**), or vehicle control (intragastrically for Entinostat control and intraperitoneally for Panobinostat control) three times per week, and tumor growth was monitored ($n = 5$/group). Experiments (**A–H**) were repeated three times, and the dot plots are shown as mean ± SD. Significance calculated with nonparametric Mann–Whitney *U* test. ns, not significant; ***, $P < 0.001$.

Hdac3 deficiency suppresses tumor growth, which is dependent on host immune responses

Panobinostat and Entinostat both suppressed the growth of MCA205 and MC38 tumors, suggesting that inhibition of one or more class I HDACs may suppress tumor growth. To explore the role of *Hdac1, 2, 3* genes on tumor growth, we knocked out *Hdac1*, *2, 3* genes in MC38 cells by CRISPR/Cas9 technology (Supplementary Fig. S1A–S1C) and injected the cells into C57BL/6 mice. Comparing the tumor growth of $Hdac1^{-/-}$, $Hdac2^{-/-}$, and $Hdac3^{-/-}$ cells with their corresponding WT MC38 tumors, we found that *Hdac3* deficiency significantly suppressed MC38 tumor growth, whereas *Hdac1* and *Hdac2* deficiency showed no obvious impact on the growth of MC38 tumors (**Fig. 2A**). To confirm the involvement of the *Hdac3* gene in tumor growth, we further knocked down ($Hdac3^{+/-}$) and

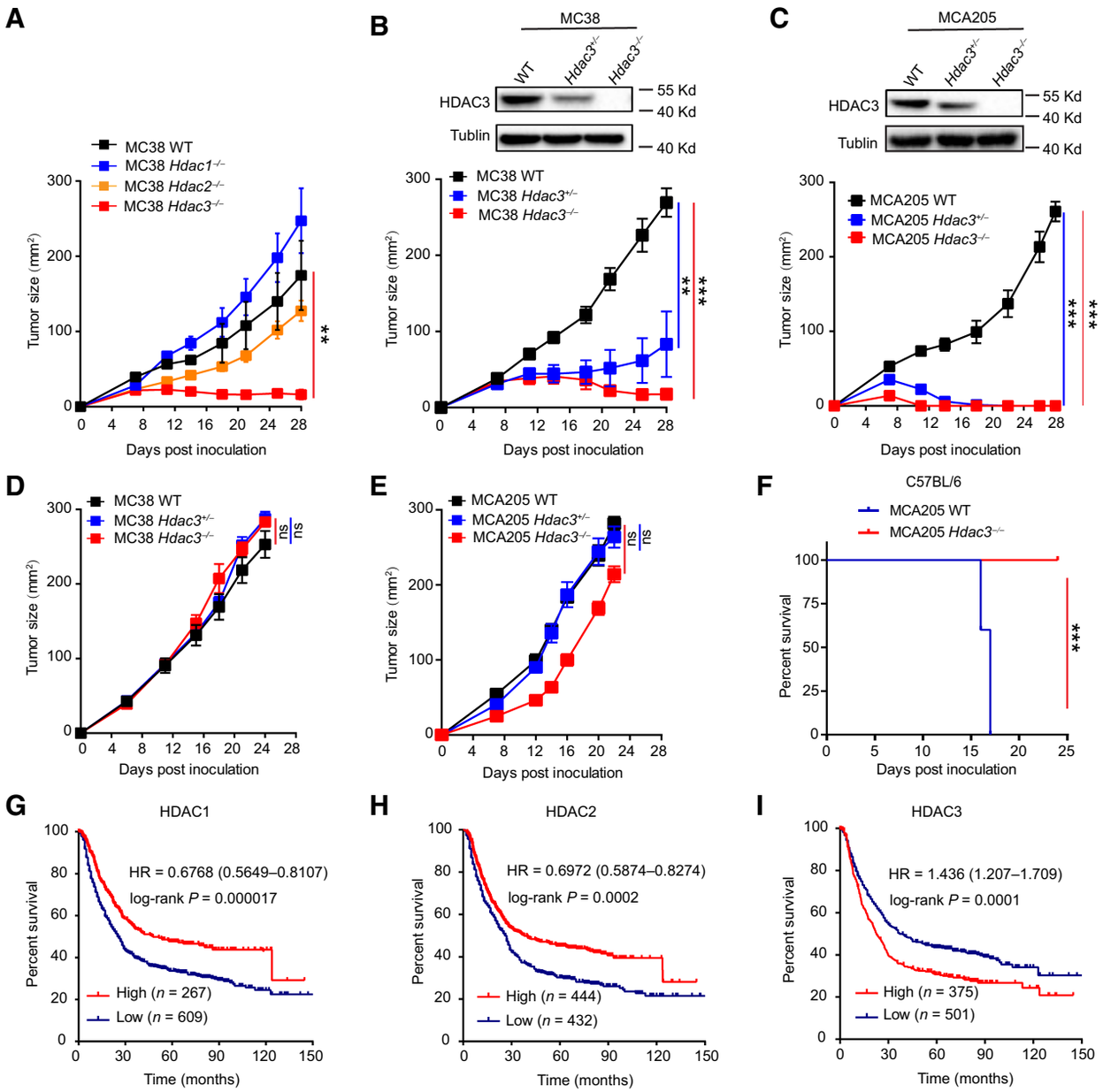

Figure 2.

Hdac3 deficiency suppresses tumor growth and is dependent on host immune responses. **A,** WT, $Hdac1^{-/-}$, $Hdac2^{-/-}$, and $Hdac3^{-/-}$ MC38 cells were inoculated in C57BL/6 mice subcutaneously, and tumor growth was monitored ($n = 5$/group). WT, $Hdac3^{+/-}$, and $Hdac3^{-/-}$ MC38 and MCA205 cells were inoculated in C57BL/6 (**B** and **C**) and nude mice (**D** and **E**) subcutaneously, and tumor growth was monitored ($n = 5$/group). *Hdac3* knockdown and knockout was confirmed via Western blot analysis (top, **B** and **C**). **F,** WT and $Hdac3^{-/-}$ MCA205 cells were injected into C57BL/6 mice intravenously, and the OS of mice was monitored ($n = 8$/group). **G–I,** The OS of patients with gastric cancer was compared between individuals bearing tumors with high or low *Hdac1, 2, 3* mRNA transcription. HR, 95% confidence interval, and *P* value from the log-rank test are shown. Western blot images (**B** and **C**) are presentative results from three independent experiments. Experiments (**A–F**) were repeated two times, and the dot plots (**A–E**) are shown as mean ± SD. Significance was calculated with nonparametric Mann–Whitney *U* test. ns, not significant; **, $P < 0.01$; ***, $P < 0.001$.

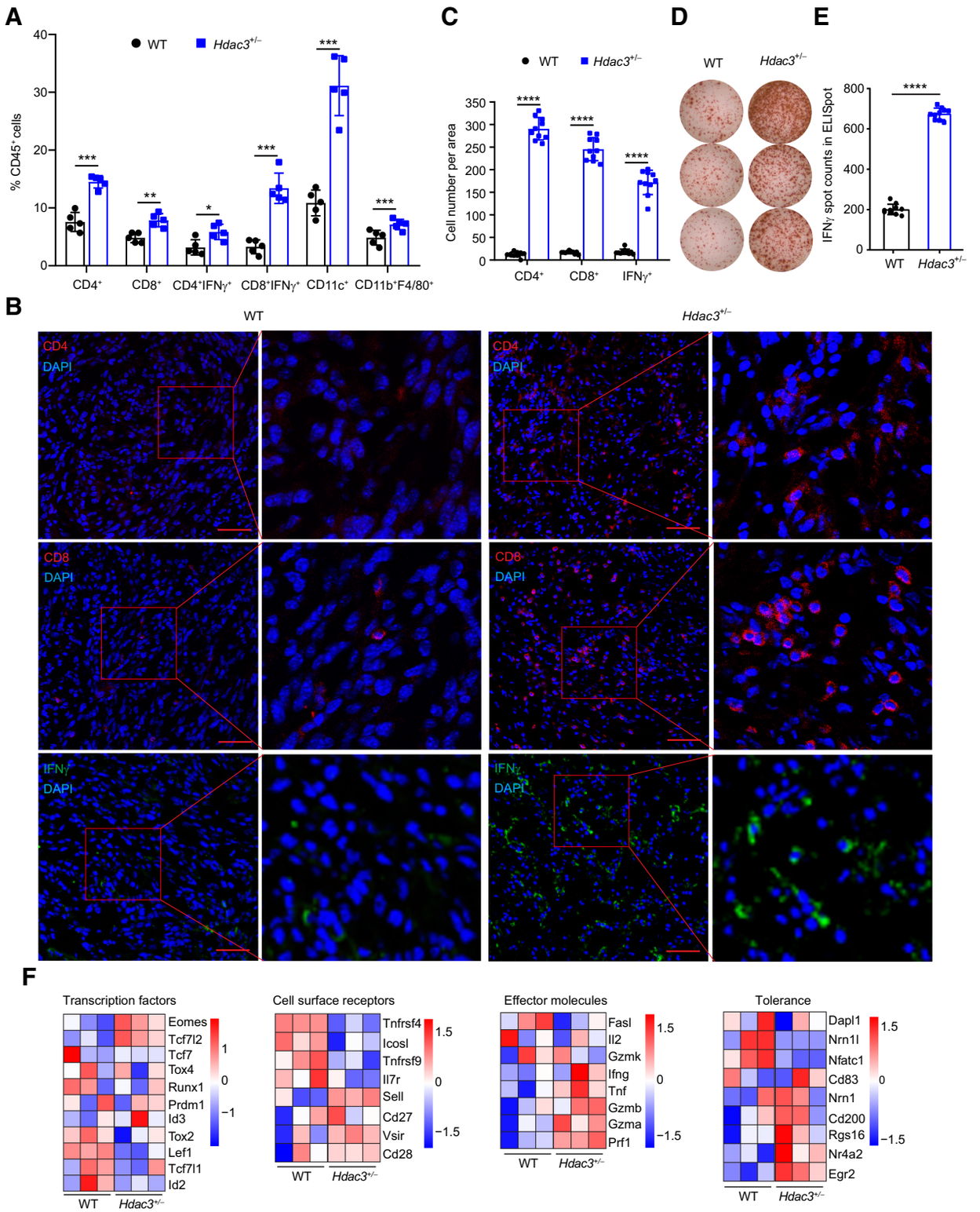
A
WT
Hdac3+/–
% CD45+ cells
CD4+
CD8+
CD4+IFNγ+
CD8+IFNγ+
CD11c+
CD11b+F4/80+
C
Cell number per area
IFNγ+
D
E
IFNγ spot counts in ELISpot
B
CD4
CD8
IFNγ
DAPI
F
Transcription factors
Eomes
Tcf7l2
Tcf7
Tox4
Runx1
Prdm1
Id3
Tox2
Lef1
Tcf7l1
Id2
Cell surface receptors
Tnfrsf4
Icosl
Tnfrsf9
Il7r
Sell
Cd27
Vsir
Cd28
Effector molecules
Fasl
Il2
Gzmk
Ifng
Tnf
Gzmb
Gzma
Prf1
Tolerance
Dapl1
Nrn1l
Nfatc1
Cd83
Nrn1
Cd200
Rgs16
Nr4a2
Egr2

knocked out (*Hdac3*$^{-/-}$) the *Hdac3* gene in MC38 and MCA205 cells. Comparing the tumor growth of *Hdac3*$^{+/-}$ and *Hdac3*$^{-/-}$ MC38 and MCA205 tumors with their corresponding WT tumors in C57BL/6 and nude mice, we found that both *Hdac3* knockdown and knockout prominently suppressed MC38 and MCA205 tumor growth in C57BL/6 mice (**Fig. 2B** and **C**), but not in nude mice (**Fig. 2D** and **E**). These results indicate that HDAC3 promotes tumor growth and is dependent on host immune responses.

After intravenous injection of MCA205 cells into the mice, tumors will develop and metastasize to multiple organs, leading to the death of mice. We then compared the survival rates of C57BL/6 mice intravenously injected with WT or *Hdac3*$^{-/-}$ MCA205 cells. Mice xenografted with WT MCA205 cells did not survive beyond 17 days after transplantation, whereas all mice xenografted with *Hdac3*$^{-/-}$ MCA205 cells survived (**Fig. 2F**), suggesting that *Hdac3* deletion reduced metastasis and protected mice from metastasis-related death. We then also analyzed the correlation of *Hdac1, 2, 3* gene expression with the OS of 876 patients with gastric cancer in GEO and TCGA databases. Higher expression of *Hdac3* gene correlated with lower OS of gastric patients, whereas higher expression of *Hdac1* and *Hdac2* genes correlated with higher OS of gastric patients (**Fig. 2G–I**). In addition, higher mRNA expression of *HDAC3* was found in various cancers tissues compared with their corresponding normal tissues, including in cholangiocarcinoma, cervical squamous cell carcinoma and endocervical adenocarcinoma, lung adenocarcinoma, lung squamous cell carcinoma (Supplementary Fig. S2). These results suggest that specific inhibition of *Hdac3* may suppress tumor growth through antitumor immunity.

Enhanced local immune responses in *Hdac3*-deficient tumors

CCK-8 (Supplementary Fig. S3A and S3B), Ki-67 staining (Supplementary Fig. S3C and S3D), and single clone formation (Supplementary Fig. S3E and S3F) assays showed that *Hdac3* deficiency had no impact on the viability and proliferation of MC38 and MCA205 cells. To explore whether HDAC3 played a role in regulating the local TME, we analyzed the tumor-infiltrating lymphocytes (TIL) in WT and *Hdac3*$^{+/-}$ MCA205 tumors by flow cytometry because *Hdac3*$^{-/-}$ cells did not form large enough tumors for flow cytometry analysis. Indeed, we observed increased number of tumor-infiltrating CD4$^+$, CD8$^+$, CD11c$^+$, CD11b$^+$F4/80$^+$, CD4$^+$IFNγ$^+$, and CD8$^+$IFNγ$^+$ immune cells in *Hdac3*$^{+/-}$ MCA205 tumors (**Fig. 3A**; Supplementary Fig. S4). The results indicate that more antigen-presenting DCs and tumor-killing T cells are recruited into MCA205 TME when *Hdac3* is deficient specifically in tumor cells. To better enumerate the magnitude and distribution of tumor-infiltrating T cells, immunofluorescence staining of WT, *Hdac3*$^{+/-}$, and *Hdac3*$^{-/-}$ MCA205 tumors was performed. A higher number of CD4$^+$, CD8$^+$, and IFNγ$^+$ cells infiltrating *Hdac3*$^{+/-}$ and *Hdac3*$^{-/-}$ MCA205 tumors compared with WT MCA205 tumors (**Fig. 3B** and **C**; Supplementary Fig. S5A and S5B). ELISpot assays were also performed to evaluate frequencies of OVA-specific IFNγ-secreting T cells in WT and *Hdac3*$^{+/-}$ MCA205 tumors stably expressing chicken OVA. The results showed that there were more IFNγ-secreting T cells in *Hdac3*$^{+/-}$ MCA205 tumors than that in WT tumors (**Fig. 3D** and **E**). These results indicate that the quantity and characterization of tumor-infiltrating T cells in *Hdac3*-deficient tumors are significantly different from that in WT tumors.

To characterize the signature of infiltrating T cells in TME, we isolated CD45$^+$CD4$^+$ and CD45$^+$CD8$^+$ T cells from WT and *Hdac3*$^{+/-}$ MCA205 tumors by FACS and performed bulk RNA-seq to detect gene expression. T cells isolated from *Hdac3*$^{+/-}$ tumors expressed higher levels of transcription factors such as *Eomes* and *Tcf712;* cell surface receptors such as *Sell*, *Vsir*, and *Cd28;* effector molecules such as *Gzmb*, *Ifng*, Prf1, and *Tnf;* and tolerance-related genes such as *Nr4a2* and *Egr2* than WT cells (**Fig. 3F**). The results above suggest that specific *Hdac3* deficiency in tumor cells triggers differential infiltration of immune cells and stronger local immune responses in TME than that in WT tumors.

Hdac3 deficiency upregulates chemokine signaling and T-cell receptor signaling pathways

Bulk RNA-seq results (**Fig. 3F**) showed that HDAC3 may impact tumor growth by regulating infiltration and signature of immune cells (especially T cells) in TME. To explore the mechanism responsible for HDAC3 regulating T-cell infiltration and the TME, we performed RNA-seq with WT and *Hdac3*$^{+/-}$ MCA205 tumor tissues. Kyoto Encyclopedia of Genes and Genomes (KEGG) annotated classification analysis comparing differential expression between *Hdac3*$^{+/-}$ and WT tumors showed that *Hdac3* deficiency significantly upregulated genes in the chemokine signaling pathway, T-cell receptor (TCR) signaling pathway, and cytokine–cytokine receptor interaction process (**Fig. 4A** and **B**). GSEA also showed that chemokine signaling (**Fig. 4C**), cytokine–cytokine receptor interaction (**Fig. 4D**), and TCR signaling pathways (**Fig. 4E**) were significantly enriched in *Hdac3*-deficient MCA205 tumors. These results suggest that TCR signaling and chemokine signaling pathways, in relation to T-cell recruitment, may contribute to the tumor growth suppression of *Hdac3*-deficient MCA205 cells. We then selected genes associated with T cells and T-cell recruitment and assessed their relative expression in WT and *Hdac3*$^{+/-}$ MCA205 tumors. Abundant T-cell markers (*Cd3d, Cd3e, Cd3g, Cd4, Cd8a, Ctla4, Zap70*, and *Cxcr3*) and T cell recruitment–related genes (*Cxcl9, 10, 11*) were significantly upregulated in *Hdac3*-deficient tumors (**Fig. 4F**). To confirm the RNA-seq results, gene expression in *Hdac3*$^{-/-}$ MCA205 tumors was compared with WT tumors via qRT-PCR. We confirmed that *Hdac3* deficiency led to upregulated T-cell marker– and T-cell recruitment–related genes (Supplementary Fig. S5C). These results led us to hypothesize that HDAC3 may suppress T-cell recruitment into TME by reducing the expression of chemokines such as *Cxcl9, 10, 11*.

HDAC3 downregulates the expression of IFN-induced chemokines *Cxcl9, 10, 11*

Chemokines *Cxcl9, 10, 11* are IFN-inducible genes, and the IFN signaling pathway plays an important role in antitumor immune responses. We therefore quantitated the mRNA expression of *Cxcl9,*

Figure 3.

Enhanced local immune response in *Hdac3*-deficient tumors. **A** and **B,** Flow cytometric analysis of immune cell infiltration in WT and *Hdac3*$^{+/-}$ MCA205 tumors. WT and *Hdac3*$^{+/-}$ MCA205 cells were inoculated in C57BL/6 mice subcutaneously (n = 5/group). Seven days after inoculation, tumor tissues were harvested, and immune cell infiltration in the tumors was analyzed by flow cytometry (**A**) and immunofluorescence staining with CD4, CD8, and IFNγ antibodies (**B**). Scale bar, 50 μm. Red box indicates area in zoomed image (10× magnification). **C,** Cumulative data and statistical analysis of **B**. ELISpot analysis of IFNγ secretion by tumor-infiltrating T lymphocytes in OVA-MCA205 and OVA-*Hdac3*$^{+/-}$ MCA205 tumors (**D**) and cumulative quantitative data (**E**). **F,** Expression of genes associated with the indicated classifications in CD45$^+$CD4$^+$ and CD45$^+$CD8$^+$ T cells isolated from WT and *Hdac3*$^{+/-}$ MCA205 tumors (n = 3/group) as analyzed by bulk RNA-seq. Flow cytometric (**A**), immunofluorescence staining (**B** and **C**), and ELISpot (**D** and **E**) assays were repeated three times, and statistical data (**A**, **C**, and **E**) are shown as mean ± SD and statistically analyzed by Mann–Whitney U test. *, $P < 0.05$; **, $P < 0.01$; ***, $P < 0.001$; and ****, $P < 0.0001$.

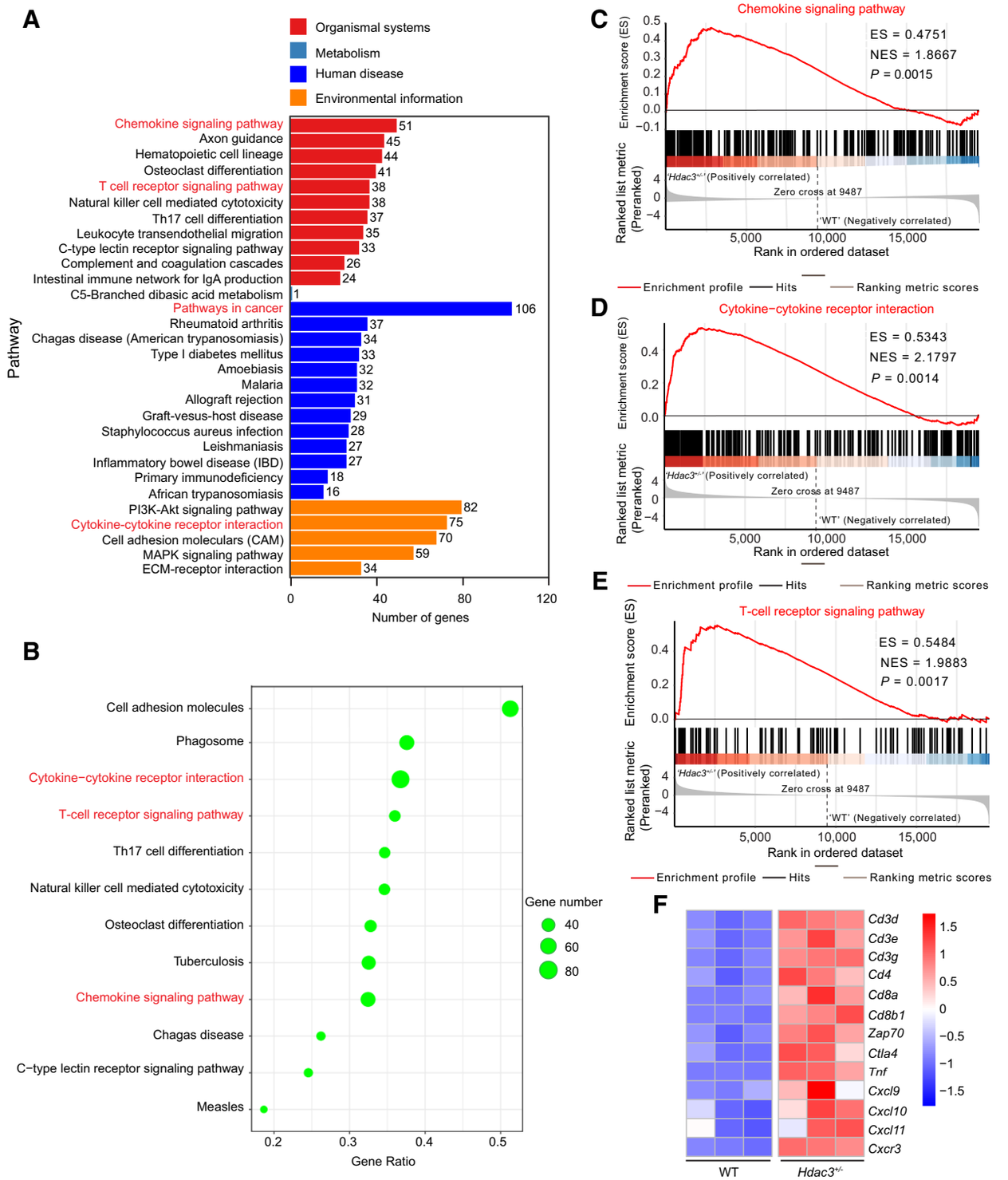

Figure 4.

Hdac3 deficiency upregulates chemokine signaling and TCR signaling pathways. **A–F,** Total RNA from WT or *Hdac3*$^{+/-}$ MCA205 tumors ($n = 3$/group) was extracted and sequenced by RNA-seq. Expression changes in *Hdac3*$^{+/-}$ versus WT MCA205 whole tumors were compared by KEGG analysis (**A** and **B**). Significantly enriched KEGG annotated classification bar chart (**A**) and distribution point map (**B**) are shown. Expression changes in *Hdac3*$^{+/-}$ versus WT MCA205 tumors were compared by GSEA (**C–E**). Chemokine signaling (**C**), cytokine–cytokine receptor interaction (**D**), and TCR signaling pathways (**E**) are shown. Heat map shows differentially expressed genes associated with the chemokine signaling pathway and T cells in WT and *Hdac3*$^{+/-}$ MCA205 tumors (**F**). The RNA-seq was performed once.

10, 11 in IFNα-, IFNβ-, and IFNγ-treated WT and *Hdac3*$^{-/-}$ MCA205 cells. qRT-PCR results showed that *Cxcl9, 10, 11* mRNAs were much higher in IFN-treated *Hdac3*$^{-/-}$ cells than in WT cells (**Fig. 5A**). Next, we quantitated the concentration of CXCL9, 10, 11 in IFNα-, IFNβ-, and IFNγ-treated WT and *Hdac3*$^{-/-}$ MCA205 cell culture supernatants by ELISA. Similar to the mRNA expression, the protein concentrations of CXCL9, 10, 11 were also higher in *Hdac3*$^{-/-}$ MCA205 cell culture supernatants than those from WT cells (**Fig. 5B**). To confirm the upregulated expression of *Cxcl9, 10, 11* in *Hdac3*$^{+/-}$ MCA205 tumors *in vivo*, we measured the concentrations of CXCL9, 10, 11 in tumors tissues by ELISA and found CXCL9, 10, 11 in *Hdac3*$^{+/-}$ MCA205 tumors were also higher than that in WT MCA205 tumors (**Fig. 5C**). These results indicate that *Hdac3* deficiency upregulates the expression of *Cxcl9, 10, 11* in tumor cells.

To further confirm the role of deacetylation enzyme activity of HDAC3 on *Cxcl9, 10, 11* expression, class I HDAC inhibitor Entinostat and HDAC3-specific inhibitor RGF966 were added into IFN-treated MCA205 cells and the mRNA expression of *Cxcl9, 10, 11* were measured by qRT-PCR. The HDAC inhibitors Entinostat and RGF966 also induced upregulation of *Cxcl9, 10, 11* mRNA expression (**Fig. 5D**). Correspondingly, we also detected upregulated expression of the CXCL9, 10, 11 receptor gene, *Cxcr3*, in *Hdac3*$^{+/-}$ MCA205 tumors (**Fig. 5E**). These results suggest that HDAC3 regulates *Cxcl9, 10, 11* mRNA expression and is dependent on its deacetylation enzyme activity.

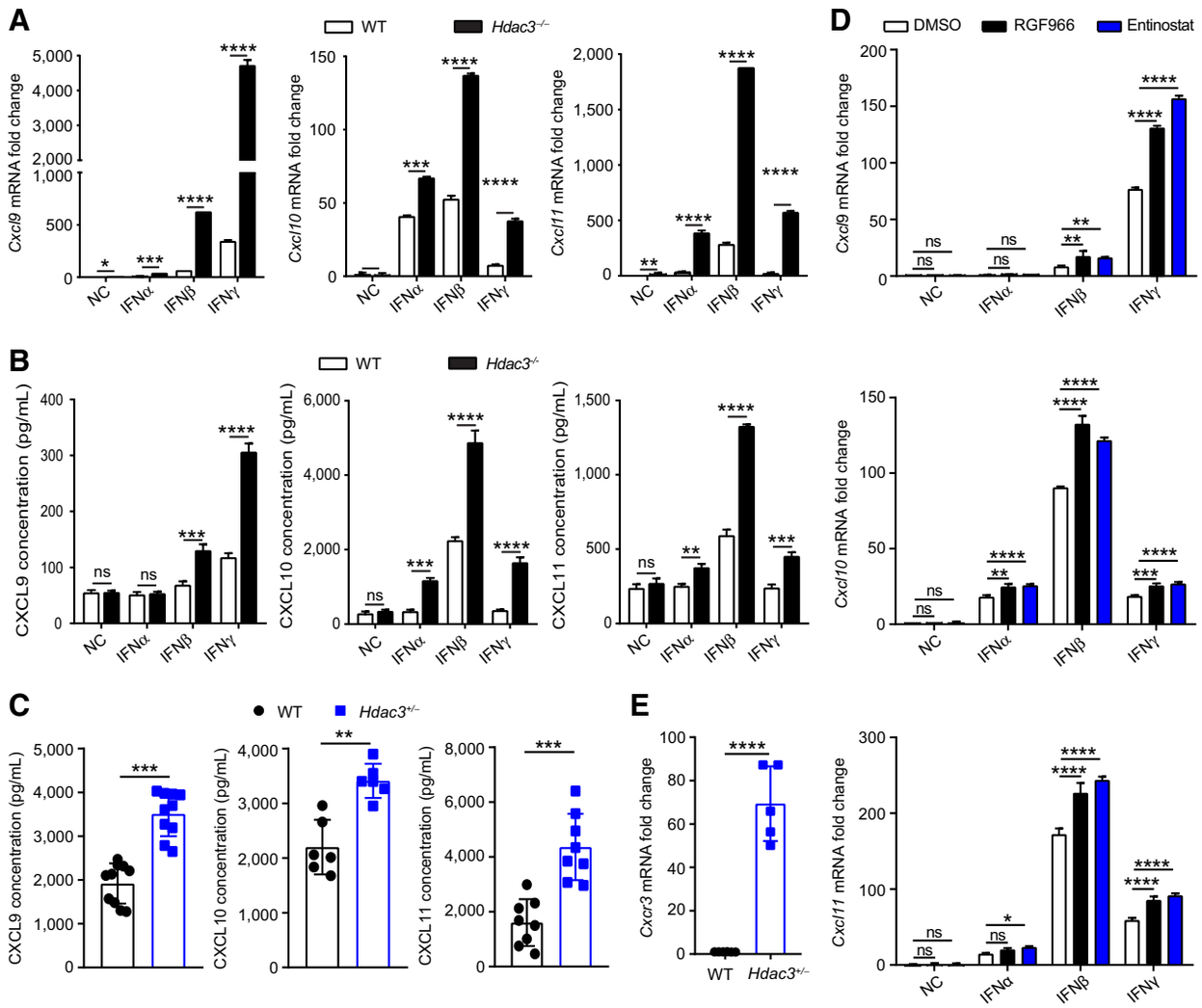

Figure 5.

HDAC3 downregulates the expression of IFN-induced chemokines *Cxcl9, 10, 11*. **A,** The mRNA expression of *Cxcl9, 10, 11* in WT and *Hdac3*$^{-/-}$ MCA205 cells treated with IFNα (100 U/mL), IFNβ (10 ng/mL), and IFNγ (100 U/mL) for 6 hours analyzed by qRT-PCR. **B,** CXCL9, 10, 11 concentrations from WT and *Hdac3*$^{-/-}$ MCA205 cell culture supernatants were measured by ELISA. **C,** CXCL9, 10, 11 concentrations in WT ($n \geq 6$) and *Hdac3*$^{+/-}$ ($n \geq 6$) MCA205 tumors were measured by ELISA. **D,** The mRNA expression of *Cxcl9, 10, 11* in WT and *Hdac3*$^{-/-}$ MCA205 cells treated with RGF966 (10 μmol/L), Entinostat (10 μmol/L), or DMSO control for 6 hours analyzed by qRT-PCR. **E,** The mRNA expression of *Cxcr3* in WT and *Hdac3*$^{+/-}$ MCA205 tumors analyzed by qRT-PCR ($n = 5$/group). qRT-PCR (**A**, **D**, and **E**) and ELISA (**B** and **C**) assays were repeated three times, and data are shown as mean ± SD. Significance was calculated with nonparametric Mann–Whitney *U* test. ns, not significant; *, $P < 0.05$; **, $P < 0.01$; ***, $P < 0.001$; and ****, $P < 0.0001$. NC; negative control.

HDAC3 directly binds and deacetylates the *Cxcl10* gene promotor

We next tried to explore the mechanism by which HDAC3 regulated the expression of *Cxcl9, 10, 11*. First, we compared the relative expression of *Cxcl9, 10, 11* mRNA in IFNα-, IFNβ-, and IFNγ-treated versus untreated MCA205 cells. The expression of *Cxcl10* was higher than *Cxcl9* and *Cxcl11* in MCA205 cells (Supplementary Fig. S6A and S6B), suggesting that CXCL10 is the main chemokine responsible for $CXCR3^+$ T-cell recruitment in MCA205 tumors. HDAC3 is an epigenetic regulator that can mediate the deacetylation modification of histones. We next performed ChIP-seq and ChIP-qPCR assays to examine the enrichment of HDAC3 and H3K27 acetylation (H3K27ac) on the *Cxcl10* promotor. HDAC3 was enriched at *Cxcl10* promotor region, and the H3K27ac levels were low in untreated and IFNβ-stimulated WT MCA205 cells. However, the enrichment of HDAC3 on *Cxcl10* promotor was reduced in $Hdac3^{+/-}$ and $Hdac3^{-/-}$ MCA205 cells, and the H3K27ac levels were increased after IFNβ stimulation (**Fig. 6A–D**). These results suggest that HDAC3 can bind to and suppress H3K27ac of the *Cxcl10* promotor. To further determine the effects of the HDAC3 deacetylation enzyme activity on *Cxcl10* transcription, we reconstituted $Hdac3^{-/-}$ MCA205 cells with WT and deacetylation inactive mutant HDAC3 (H134/135Q; Supplementary Fig. S7A and S7B). CCK-8 (Supplementary Fig. S7C), Ki-67 staining (Supplementary Fig. S7D), and single clone formation assay (Supplementary Fig. S7E and S7F) showed that *Hdac3* overexpression had no impact on the viability and proliferation of MCA205 cells. Furthermore, ChIP-qPCR and ChIP-seq results showed that WT HDAC3 but not HDAC3 H134/135Q mutant could bind to and suppress the acetylation of the *Cxcl10* promotor (**Fig. 6E–H**). Further analysis on *Cxcl10* mRNA expression in $Hdac3^{-/-}$ MCA205 cells reconstituted with WT and mutant HDAC3 also showed that WT HDAC3 suppressed *Cxcl10* mRNA expression, whereas H134/135Q-mutant HDAC3 had no impact on *Cxcl10* mRNA expression (**Fig. 6I**). Furthermore, we then inoculated $Hdac3^{-/-}$ MCA205 cells reconstituted with vector, WT, or H134/135Q-mutant HDAC3 in C57BL/6 and nude mice. Tumor growth monitoring showed that WT, but not H134/135Q mutant, HDAC3 rescued tumor growth in $Hdac3^{-/-}$ cells in C57BL/6 mice, but not in nude mice (**Fig. 6J** and **K**). These results suggest that HDAC3 suppresses *Cxcl10* gene expression by binding the *Cxcl10* promotor and deacetylating nearby histones.

CXCR3 antibody blocking rescues *Hdac3*-deficient MCA205 tumor growth in an immune-dependent manner

To further test the hypothesis that *Hdac3* deficiency promoted the recruitment of $CXCR3^+$ T cells to mediate antitumor immune responses, we used a CXCR3 antibody to block the CXCL9, 10, 11/CXCR3 chemokine signaling pathway in WT and $Hdac3^{+/-}$ MCA205 tumors. Although the TNFα antibody and IgG had no effects on the slow growth of $Hdac3^{+/-}$ MCA205 tumors, CXCR3 antibody restored the growth of $Hdac3^{+/-}$ MCA205 tumors to a similar rate as WT MCA205 tumors (**Fig. 7A**). Further analysis of the TILs in WT, IgG-treated, or CXCR3 antibody–treated $Hdac3^{+/-}$ MCA205 tumors by flow cytometry showed that $CD4^+$, $CD8^+$, $CXCR3^+$, $CD4^+CXCR3^+$, and $CD8^+CXCR3^+$ infiltrating immune cells were decreased in $Hdac3^{+/-}$ MCA205 tumors after CXCR3 antibody administration (**Fig. 7B**). Similarly, decreased $CD4^+$, $CD8^+$, and $IFN\gamma^+$ cell numbers were observed in immunofluorescence staining of $Hdac3^{+/-}$ MCA205 tumors with CXCR3 antibody administration compared with IgG administration group (**Fig. 7C** and **D**). *Cxcr3* mRNA was also decreased in CXCR3 antibody–treated $Hdac3^{+/-}$ MCA205 tumors, which was likely due to reduced infiltration of *Cxcr3*-expressing T cells (**Fig. 7E**). These results suggest that reduced growth of *Hdac3*-deficient tumors is likely due to enhanced antitumor activity mediated by $CXCR3^+$ T cells infiltrating into the TME. Overall, our studies suggest HDAC3 is involved in antitumor immunity by regulating the expression of *Cxcl9, 10, 11* genes and CXCL9, 10, 11-CXCR3 axis–mediated T-cell recruitment in TME, providing a vital anti-tumor mechanism of HDAC3 inhibition (**Fig. 7F**).

We additionally inoculated MTX-treated WT, $Hdac3^{+/-}$ or $Hdac3^{-/-}$ MCA205 cells into the right side of mice with WT MCA205 tumors on the left side for 7 days, we found that MTX-treated $Hdac3^{+/-}$ and $Hdac3^{-/-}$ MCA205 cells inoculation on one side suppress the tumor growth of WT MCA205 tumors on the other side (Supplementary Fig. S8A and S8B), indicating that *Hdac3*-deficient MCA205 cells have distal antitumor activity *in vivo*. To determine the contribution of the CXCL10/CXCR3 axis in the antitumor activity of *Hdac3*-deficient MCA205 cells, we inoculated WT, $Hdac3^{+/-}$ or $Hdac3^{-/-}$ MCA205 fibrosarcoma cells into the right side of mice xenografted with WT MCA205 tumors on the left side for 7 days, and then intravenously administrated these mice with CXCR3 antibody or IgG control. CXCR3 antibody restored MCA205 tumor growth (Supplementary Fig. S8C), suggesting that the antitumor activity of *Hdac3* deficient cells *in vivo* is dependent on the CXCL10 and CXCR3 pathway.

HDAC3 expression inversely correlates with CXCL10 in the TME of human HCC

To validate the regulation relationship between HDAC3 and CXCL10 in human samples, we collected malignant ($n = 86$) and benign tissues ($n = 41$) of patients with HCC and performed TMA-IHC to evaluate the protein expression of HDAC3, CD8a, CXCL10, and CXCR3 (Supplementary Tables S1 and S2). HDAC3 expression was elevated in cancerous tissues compared with benign tissues, whereas CXCL10 was lower in cancerous tissues than in benign tissues (Supplementary Fig. S9A and S9B). Furthermore, when the clinical outcomes of different subgroups classed by HDAC3 and CXCL10 levels were analyzed by Kaplan–Meier analysis, the results indicated that patients with HCC with higher HDAC3 or lower CXCL10 expression (cutoff = 50%) showed worse prognosis than patients with HCC with lower HDAC3 or higher CXCL10 expression (Supplementary Fig. S9C). To observe the relationship between HDAC3, CXCL10, CD8a, and CXCR3 in HCC samples, we then further analyzed the correlation between HDAC3, CD8a, CXCL10, and CXCR3 levels. Protein levels of HDAC3 were modest but exhibited a significant inverse correlation with the expression of CD8a and CXCL10, and the expression of CD8a positively correlated with the protein levels of CXCR3 (Supplementary Fig. S9D). These results from clinical samples indicate that HDAC3 may regulate the expression of CXCL10 and further affect the infiltration of $CD8^+$ T cells in TME of HCC.

Discussion

HDAC inhibitors have been increasingly used as therapeutic drugs to treat many kinds of cancers and other diseases. However, the mechanisms responsible for their chemotherapeutic actions are not fully understood. Commonly, HDAC inhibitors are thought to exert antitumor activity by causing cell-cycle arrest, inhibiting DNA repair, inducing apoptosis, and altering gene expression by acetylating non-histone proteins (4, 5, 24). In this study, we found that class I HDAC inhibitors, Entinostat and Panobinostat, suppressed MCA205 and

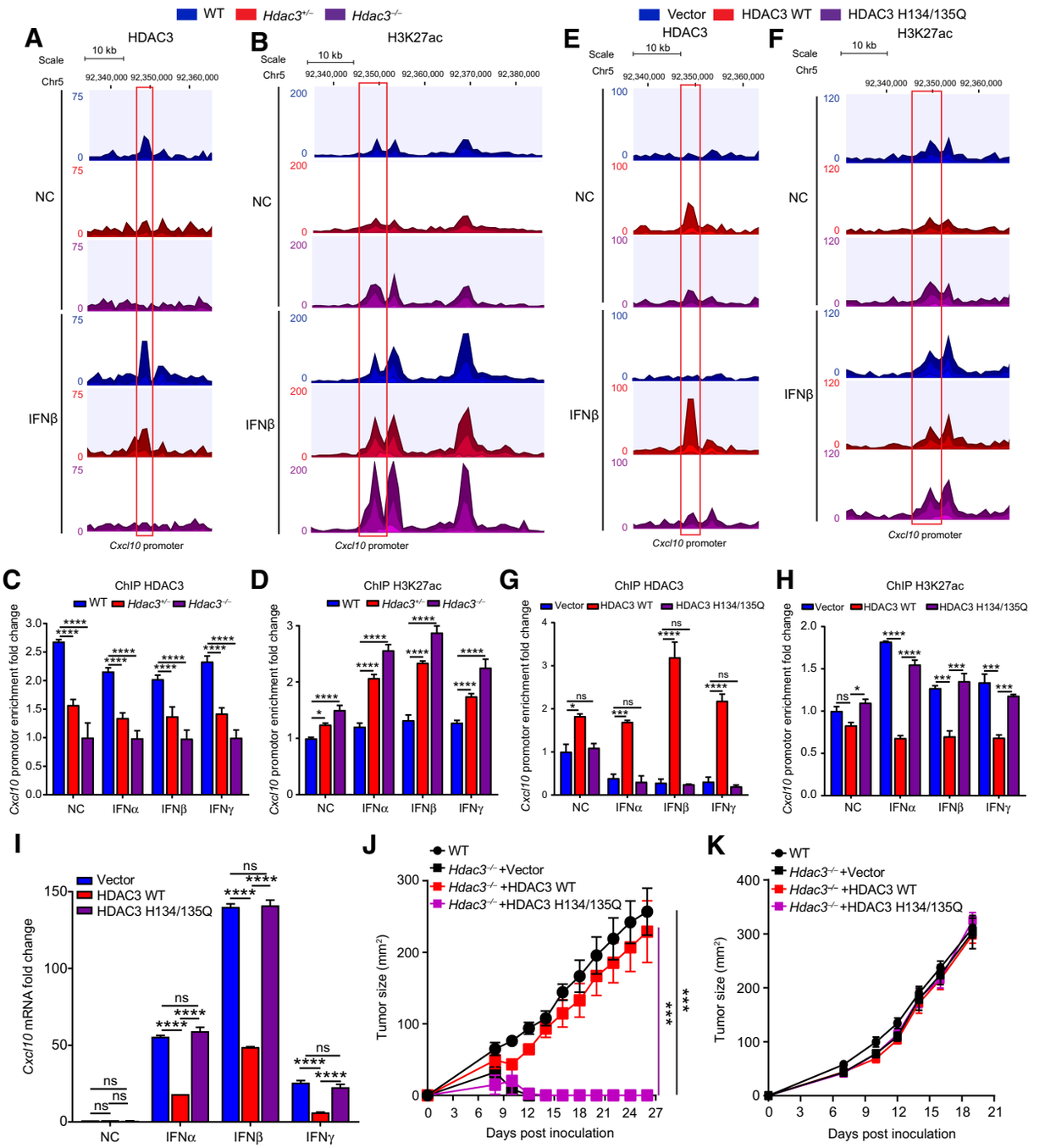

Figure 6.

HDAC3 directly binds and deacetylates *Cxcl10* gene promotor. **A** and **B,** The *Cxcl10* gene promotor loci are displayed. Tracks depict HDAC3 ChIP (**A**) signal, as well as ChIP for H3K27ac (**B**) in WT, *Hdac3*$^{+/-}$, and *Hdac3*$^{-/-}$ MCA205 cells treated with IFNβ (10 ng/mL) or vehicle control treatment for 3 hours. *Cxcl10* promotor occupancy of HDAC3 (**C**) and H3K27ac (**D**) proteins in WT, *Hdac3*$^{+/-}$, and *Hdac3*$^{-/-}$ MCA205 cells analyzed by ChIP q-PCR. **E** and **F,** The *Cxcl10* gene promotor loci are displayed. Tracks depict HDAC3 ChIP (**E**) signal, as well as ChIP for H3K27ac (**F**) in *Hdac3*$^{-/-}$ MCA205 cells overexpressing WT or H134/135Q mutant HDAC3, or vector control. *Cxcl10* promotor occupancy of HDAC3 (**G**) and H3K27ac (**H**) proteins in *Hdac3*$^{-/-}$ MCA205 cells overexpressing WT or H134/135Q-mutant HDAC3, or vector control as analyzed by ChIP q-PCR. **I,** The mRNA expression of *Cxcl10* in *Hdac3*$^{-/-}$ MCA205 cells overexpressing WT, H134/135Q mutant HDAC3 or vector control as analyzed by qRT-PCR. MCA205 cells were treated with 100 U/mL IFNα, 10 ng/mL IFNβ, or 100 U/mL IFNγ for 6 hours before being lysed for RNA extraction. **J–K,** WT MCA205 and vector control, WT and H134/135Q-mutant HDAC3 overexpressing *Hdac3*$^{-/-}$ MCA205 cells were inoculated in C57BL/6 mice or nude mice subcutaneously (n = 5/group), and tumor growth was monitored. ChIP q-PCR (**C**, **D**, **G**, **H**) and qRT-PCR (**I**) were repeated two times, and data are shown as mean ± SD. Experiments (**J** and **K**) were repeated two times, and the dot plots are shown as mean ± SD. Significance was calculated with nonparametric Mann–Whitney U test. ns, not significant; *, $P < 0.05$; ***, $P < 0.001$; and ****, $P < 0.0001$. NC; negative control.

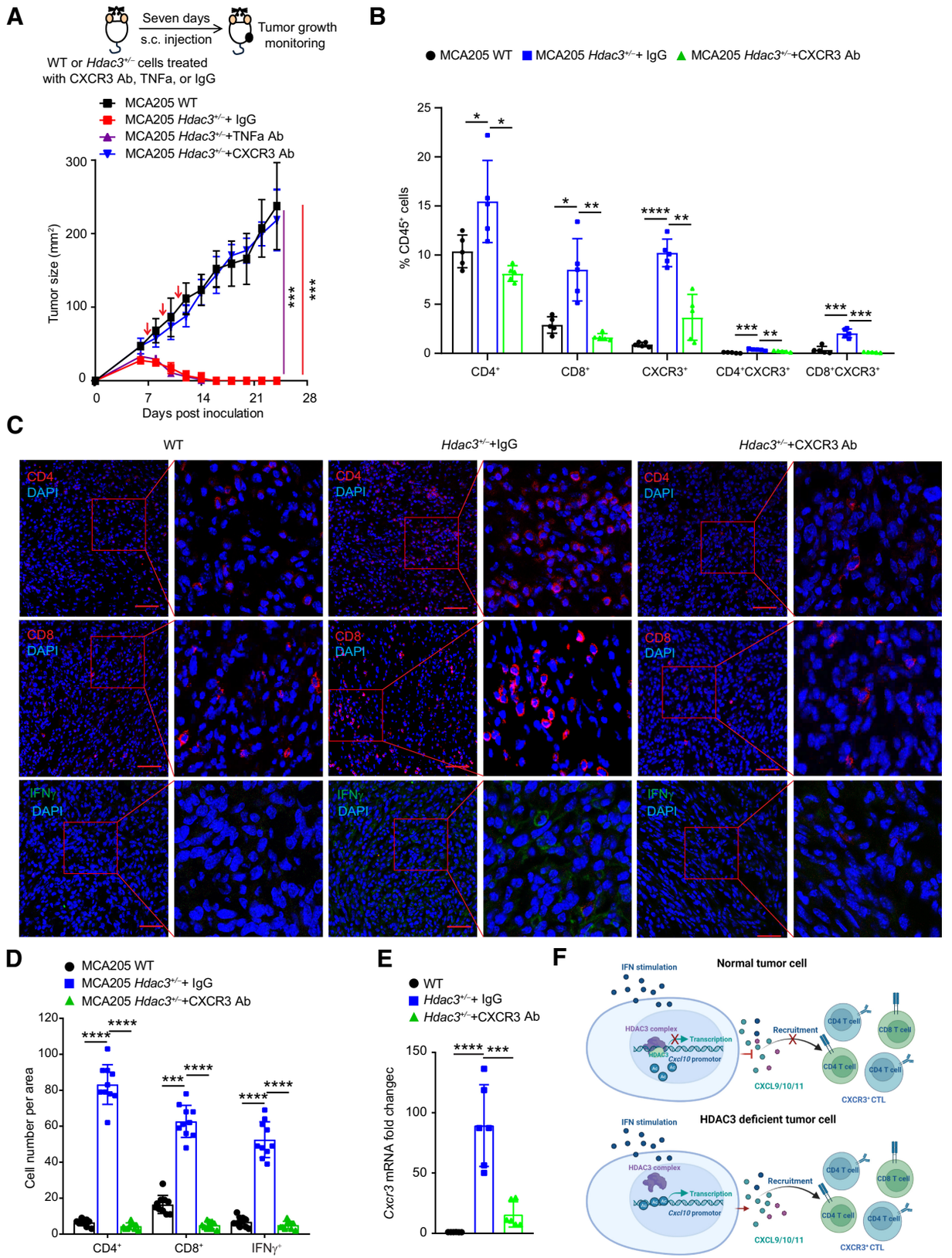
A
Seven days
s.c. injection
Tumor growth
monitoring
WT or Hdac3+/− cells treated
with CXCR3 Ab, TNFa, or IgG
MCA205 WT
MCA205 Hdac3+/−+ IgG
MCA205 Hdac3+/−+TNFa Ab
MCA205 Hdac3+/−+CXCR3 Ab
Tumor size (mm2)
Days post inoculation
B
MCA205 WT
MCA205 Hdac3+/−+ IgG
MCA205 Hdac3+/−+CXCR3 Ab
% CD45+ cells
CD4+
CD8+
CXCR3+
CD4+CXCR3+
CD8+CXCR3+
C
WT
Hdac3+/−+IgG
Hdac3+/−+CXCR3 Ab
CD4
CD8
IFNγ
DAPI
D
MCA205 WT
MCA205 Hdac3+/−+ IgG
MCA205 Hdac3+/−+CXCR3 Ab
Cell number per area
CD4+
CD8+
IFNγ+
E
WT
Hdac3+/−+ IgG
Hdac3+/−+CXCR3 Ab
Cxcr3 mRNA fold changec
F
Normal tumor cell
IFN stimulation
HDAC3 complex
Transcription
Cxcl10 promotor
Recruitment
CD4 T cell
CD8 T cell
CXCL9/10/11
CXCR3+ CTL
HDAC3 deficient tumor cell

MC38 tumors in immunocompetent but not in immunodeficient nude mice, suggesting that they conduct antitumor activity in an immune-dependent manner. However, it is worth noting that the immune-dependent effects of HDAC inhibitors we observed may depend upon the specific cell lines we used and the experimental setting within our models. Some research shows that HDAC inhibitors suppress tumor growth in immunodeficient mice (36, 37). This inconsistency with our results may result from different cell line usage and inhibitor administration (including dosages, times, and manners). The immune-dependent tumor suppression of HDAC inhibitors in this study may not represent the antitumor effects of other HDAC inhibitors and other tumor types. By comparing the tumor growth rates of *Hdac1, 2, 3* knockout cells in syngeneic C57BL/6 mice and nude mice, we found HDAC3 was specifically involved in regulating antitumor immunity. *Hdac3* deficiency resulted in significantly more cytotoxic and tumor-killing immune cells infiltrating into the TME than WT tumors, causing enhanced antitumor immune responses. Our studies therefore uncovered the function of HDAC3 in promoting tumor growth by suppressing tumor-killing immune cell infiltration into the TME.

Immune cell infiltration into the TME influences tumorigenesis and clinical outcome. The CXCL9, 10, 11/CXCR3 axis regulates immune responses in TME by controlling immune cell recruitment and promoting Th1 polarization (25, 38). The current work found more robust antitumor immune reactions in *Hdac3*-deficient tumors. More CTLs and $CXCR3^+$ immune cells were distributed in *Hdac3*-deficient tumors because of upregulation of the CXCL9, 10, 11/CXCR3 axis. Because CXCR3 blocking antibody restored $Hdac3^{+/-}$ tumor growth to a similar rate as $Hdac3^{+/+}$ tumors, we hypothesize that the growth inhibition of $Hadc3^{+/-}$ tumors was caused by increased expression of *Cxcl9, 10, 11* chemokines and enhanced recruitment of $CXCR3^+$ T cells into the TME, which is consistent with previous studies that indicate CXCL9, 10, 11/CXCR3 paracrine axis as a therapeutic target in cancer (39–41).

As a member of class I HDACs, HDAC3 protein is extensively expressed in various cell types and modifies different kinds of target proteins. HDAC3 interacts with NcoR1/2 and deacetylates histone and non-histone proteins, which is dependent on its deacetylation enzyme activity (8, 12, 42). A recent study shows that HDAC3 activity in the gut is upregulated by microbiota-derived inositol-1,4,5-trisphosphate to promote epithelial repair, indicating that HDAC3 acts as convergent epigenetic sensor of distinct metabolites that calibrates host responses to diverse microbial signals (43). HDAC3 is also reported to be involve in carcinogenesis of various cancer types as an epigenetic and transcriptional regulator, and HDAC3 inhibitors are effective in the treatment of many cancers (4, 11, 44, 45). HDAC3 possesses deacetylation activity–dependent and deacetylation activity–independent functions, which play different roles in physiologic processes. Nguyen and colleagues report selective enzymatic engagement of HDAC3 as a function of its differential association with NCoR1/2, selectively coordinated by either ATF3 or ATF2 during lipopolysaccharide (LPS) activation in macrophages. Deletion of HDAC3 in macrophages safeguards mice from lethal exposure to LPS, but this protection is not conferred by genetic or pharmacologic abolition of HDAC3 enzyme activity, indicating the dichotomous transcriptional activator and repressor role of HDAC3 whose noncanonical deacetylation-independent functions are vital for the innate immune system (46). HDAC3 deletion in liver upregulates lipogenic genes and results in severe hepatosteatosis (47, 48). Sun and colleagues found that pharmacologic HDAC inhibition in primary hepatocytes causes histone hyperacetylation but does not upregulate HDAC3 target gene expression. Moreover, deacetylation-dead HDAC3 mutants can rescue hepatosteatosis and repress lipogenic gene expression in HDAC3-depleted mouse liver, suggesting the deacetylation activity–independent role of HDAC3 in regulating gene transcription (49). Here, we identified the deacetylation activity–dependent epigenetic modification role of HDAC3 on *Cxcl10* gene is vital for MCA205 tumor growth.

Successful transcription of specific genes involves the orchestrated effort of transcription factors and specific enzyme protein complexes that modify chromatin structure. HDAC3 regulated *Cxcl10* gene expression by directly binding to and deacetylating the promotor of *Cxcl10* gene. These results indicate that the deacetylase activity of HDAC3 is extremely important for its function in current study. Indeed, HDAC3 enzyme activity defective mutant HDAC3 H134/135Q can neither bind to *Cxcl10* promotor nor deacetylate it. A previous report shows that H134/135 mutation leads to modest but significant reduction in most HDAC3-occupied chromatin sites (49). HDAC3 binding to different gene promotors needs not only SMRT/NcoR, but also other transcription-related factors like ATF2, ATF3, FoxO3, and Geminin (46, 50). Mutation at H134/135 sites may affect interaction of HDAC3 with other recruitment-related factors, which thus disable HDAC3 from binding to the promotor of the *Cxcl10* gene. When the deacetylase activity of HDAC3 was mutated, it cannot bind to *Cxcl10* promotor, suggesting that the deacetylase activity of HDAC3 is also engaged in the selection of chromatin sites or target proteins.

By TMA-IHC staining, we also demonstrated the inverse correlation between HDAC3 and CXCL10 protein levels in human HCC, suggesting the possible regulation relationship between HDAC3 and CXCL10 in human tumors. However, no patients with HCC treated with HDAC3 inhibitors were recruited and compared in this study. Whether HDAC3 inhibition supports antitumor immunity in human patients still remains to be investigated. In summary, we have demonstrated that HDAC3 inhibition suppresses tumor growth by promoting *Cxcl9, 10, 11* expression to recruit T-cell

Figure 7.

CXCR3 antibody blocking rescues *Hdac3*-deficient MCA205 tumor growth in an immune-dependent manner. **A,** Effect of CXCR3 or TNFα blocking on the growth of $Hdac3^{+/-}$ MCA205 tumors ($n = 6$ mice/group). Top: Schematic of experimental setup. Bottom: Tumor size was monitored. Red arrows indicate the timepoint of Ab injection. Tumor growth was monitored two to three times per week. **B** and **C,** Flow cytometric and immunofluorescence staining analysis of immune cell infiltration in WT and CXCR3 antibody–and IgG control–treated $Hdac3^{+/-}$ MCA205 tumors. WT and $Hdac3^{+/-}$ MCA205 cells were inoculated in C57BL/6 mice subcutaneously. Tumor-bearing mice were treated with CXCR3 antibody, TNFα antibody, or IgG control (10 mg/kg) by intravenous injection at 1, 3, and 5 days after inoculation. Seven days after inoculation, tumors were stripped and immune cell infiltration in tumors was analyzed by flow cytometric (**B**) and immunofluorescence staining (**C**). Scale bar, 50 μm. Red box indicates area in zoomed image (10× magnification). **D,** Statistical data of **C**. **E,** The mRNA expression of *Cxcr3* in WT and CXCR3 antibody and IgG control treated $Hdac3^{+/-}$ MCA205 tumor was analyzed by qRT-PCR ($n = 5$/group). **F,** Proposed HDAC3 pathway schematic. In tumor cells, HDAC3 deacetylated *Cxcl9/10/11* promoters and inhibited their expression. Low levels of CXCL9/10/11 cannot recruit enough $CXCR3^+$ CTL to mediate tumor killing. In Hdac3-deficient tumor cells, deficiency of HDAC3 resulted in the acetylation modification of *Cxcl9/10/11* promoters and gene expression. CXCL9/10/11 induced infiltration of $CXCR3^+$ T cells into the TME and tumor killing. All arrows indicated promotion or induction; Red "X" on arrow and red blunted line indicated inhibition. The dot plot (**A**), flow cytometry (**B**), immunofluorescence staining (**D**), and qRT-PCR (**E**) were repeated two times, and data are shown as mean ± SD. Significance was calculated with nonparametric Mann–Whitney *U* test. ns, not significant; *, $P < 0.05$; **, $P < 0.01$; ***, $P < 0.001$; and ****, $P < 0.0001$.

infiltration into TME. This work may help guide future cancer therapy by applying HDAC3-specific inhibitors in tumor cells.

Authors' Disclosures

No disclosures were reported.

Authors' Contributions

L. Li: Conceptualization, funding acquisition, investigation, writing–original draft, writing–review and editing. **S. Hao:** Investigation. **M. Gao:** Software, investigation, methodology. **J. Liu:** Investigation, methodology. **X. Xu:** Data curation, methodology. **J. Huang:** Resources, funding acquisition. **G. Cheng:** Conceptualization, resources, funding acquisition, writing–original draft, writing–review and editing. **H. Yang:** Conceptualization, resources, supervision, funding acquisition.

Acknowledgments

This project is financially supported by National Natural Science foundation of China (82102371, 82073181, 81874067, and 81802870), Chinese Academy of Medical Sciences Innovation Fund for Medical Sciences (2021-I2M-1-047), the Non-profit Central Research Institute Fund of Chinese Academy of Medical Sciences (2020-PT310-006), the Key Project of Jiangsu Provincial Health Commission (K2019021). H. Yang is supported by Natural Science foundation of Jiangsu Province (BK20211554). L. Li is supported by the Innovative and Entrepreneurial Doctor grant (2020-2022) from Jiangsu Province. We appreciate the help of animal facility and Immunology Platform at Suzhou Institute of Systems Medicine.

The publication costs of this article were defrayed in part by the payment of publication fees. Therefore, and solely to indicate this fact, this article is hereby marked "advertisement" in accordance with 18 USC section 1734.

Note

Supplementary data for this article are available at Cancer Immunology Research Online (http://cancerimmunolres.aacrjournals.org/).

Received April 22, 2022; revised September 21, 2022; accepted February 22, 2023; published first February 27, 2023.

References

1. de Ruijter AJ, van Gennip AH, Caron HN, Kemp S, van Kuilenburg AB. Histone deacetylases (HDACs): characterization of the classical HDAC family. The Biochem J 2003;370:737–49.
2. Witt O, Deubzer HE, Milde T, Oehme I. HDAC family: What are the cancer relevant targets? Cancer Lett 2009;277:8–21.
3. McClure JJ, Li X, Chou CJ. Advances and challenges of HDAC inhibitors in cancer therapeutics. Adv Cancer Res 2018;138:183–211.
4. Lakshmaiah KC, Jacob LA, Aparna S, Lokanatha D, Saldanha SC. Epigenetic therapy of cancer with histone deacetylase inhibitors. J Cancer Res Ther 2014;10:469–78.
5. Sun Y, Sun Y, Yue S, Wang Y, Lu F. Histone deacetylase inhibitors in cancer therapy. Curr Top Med Chem 2018;18:2420–8.
6. Yoon S, Eom GH. HDAC and HDAC inhibitor: from cancer to cardiovascular diseases. Chonnam Med J 2016;52:1–11.
7. Hull EE, Montgomery MR, Leyva KJ. HDAC inhibitors as epigenetic regulators of the immune system: impacts on cancer therapy and inflammatory diseases. Biomed Res Int 2016;2016:8797206.
8. Emmett MJ, Lazar MA. Integrative regulation of physiology by histone deacetylase 3. Nat Rev Mol Cell Biol 2019;20:102–15.
9. Nemati M, Ajami N, Estiar MA, Rezapour S, Gavgani RR, Hashemzadeh S, et al. Deregulated expression of HDAC3 in colorectal cancer and its clinical significance. Adv Clin Exp Med 2018;27:305–11.
10. Ji H, Zhou Y, Zhuang X, Zhu Y, Wu Z, Lu Y, et al. HDAC3 deficiency promotes liver cancer through a defect in H3K9ac/H3K9me3 transition. Cancer Res 2019;79:3676–88.
11. Cao F, Zwinderman MRH, Dekker FJ. The process and strategy for developing selective histone deacetylase 3 inhibitors. Molecules 2018;23:551.
12. Bhaskara S, Knutson SK, Jiang G, Chandrasekharan MB, Wilson AJ, Zheng S, et al. Hdac3 is essential for the maintenance of chromatin structure and genome stability. Cancer Cell 2010;18:436–47.
13. Wei H, Ma W, Lu X, Liu H, Lin K, Wang Y, et al. KDELR2 promotes breast cancer proliferation via HDAC3-mediated cell cycle progression. Cancer Commun 2021;41:904–20.
14. Mondello P, Tadros S, Teater M, Fontan L, Chang AY, Jain N, et al. Selective inhibition of HDAC3 targets synthetic vulnerabilities and activates immune surveillance in lymphoma. Cancer Discov 2020;10:440–59.
15. Jiang Y, Ortega-Molina A, Geng H, Ying HY, Hatzi K, Parsa S, et al. CREBBP inactivation promotes the development of HDAC3-dependent lymphomas. Cancer Discov 2017;7:38–53.
16. Bhaskara S, Chyla BJ, Amann JM, Knutson SK, Cortez D, Sun ZW, et al. Deletion of histone deacetylase 3 reveals critical roles in S phase progression and DNA damage control. Mol Cell 2008;30:61–72.
17. Hu G, He N, Cai C, Cai F, Fan P, Zheng Z, et al. HDAC3 modulates cancer immunity via increasing PD-L1 expression in pancreatic cancer. Pancreatology 2019;19:383–9.
18. Chen G, Yan Q, Liu L, Wen X, Zeng H, Yin S. Histone deacetylase 3 governs beta-estradiol-ERalpha-involved endometrial tumorigenesis via inhibition of STING transcription. Cancers 2022;14:4718.
19. Li Y, Liu Y, Zhao N, Yang X, Li Y, Zhai F, et al. Checkpoint regulator B7x is epigenetically regulated by HDAC3 and mediates resistance to HDAC inhibitors by reprogramming the tumor immune environment in colorectal cancer. Cell Death Dis 2020;11:753.
20. Hsieh HY, Chuang HC, Shen FH, Detroja K, Hsin LW, Chen CS. Targeting breast cancer stem cells by novel HDAC3-selective inhibitors. Eur J Med Chem 2017;140:42–51.
21. Sarkar R, Banerjee S, Amin SA, Adhikari N, Jha T. Histone deacetylase 3 (HDAC3) inhibitors as anticancer agents: a review. Eur J Med Chem 2020;192:112171.
22. Vilgelm AE, Richmond A. Chemokines modulate immune surveillance in tumorigenesis, metastasis, and response to immunotherapy. Front Immunol 2019;10:333.
23. O'Hayre M, Salanga CL, Handel TM, Allen SJ. Chemokines and cancer: migration, intracellular signalling and intercellular communication in the microenvironment. Biochem J 2008;409:635–49.
24. Schneider GP, Salcedo R, Welniak LA, Howard OM, Murphy WJ. The diverse role of chemokines in tumor progression: prospects for intervention (Review). Int J Mol Med 2001;8:235–44.
25. Tokunaga R, Zhang W, Naseem M, Puccini A, Berger MD, Soni S, et al. CXCL9, CXCL10, CXCL11/CXCR3 axis for immune activation - a target for novel cancer therapy. Cancer Treat Rev 2018;63:40–7.
26. Zhu G, Yan HH, Pang Y, Jian J, Achyut BR, Liang X, et al. CXCR3 as a molecular target in breast cancer metastasis: inhibition of tumor cell migration and promotion of host anti-tumor immunity. Oncotarget 2015;6:43408–19.
27. Franciszkiewicz K, Boissonnas A, Boutet M, Combadiere C, Mami-Chouaib F. Role of chemokines and chemokine receptors in shaping the effector phase of the antitumor immune response. Cancer Res 2012;72:6325–32.
28. Ohmori Y, Wyner L, Narumi S, Armstrong D, Stoler M, Hamilton TA. Tumor necrosis factor-alpha induces cell type and tissue-specific expression of chemoattractant cytokines *in vivo*. Am J Pathol 1993;142:861–70.
29. Ohmori Y, Schreiber RD, Hamilton TA. Synergy between interferon-gamma and tumor necrosis factor-alpha in transcriptional activation is mediated by cooperation between signal transducer and activator of transcription 1 and nuclear factor kappaB. The Journal of biological chemistry. J Biol Chem 1997;272:14899–907.
30. Muehlinghaus G, Cigliano L, Huehn S, Peddinghaus A, Leyendeckers H, Hauser AE, et al. Regulation of CXCR3 and CXCR4 expression during terminal differentiation of memory B cells into plasma cells. Blood 2005;105:3965–71.
31. Zhang R, Tian L, Chen LJ, Xiao F, Hou JM, Zhao X, et al. Combination of MIG (CXCL9) chemokine gene therapy with low-dose cisplatin improves therapeutic efficacy against murine carcinoma. Gene Ther 2006;13:1263–71.

32. Pradelli E, Karimdjee-Soilihi B, Michiels JF, Ricci JE, Millet MA, Vandenbos F, et al. Antagonism of chemokine receptor CXCR3 inhibits osteosarcoma metastasis to lungs. Int J Cancer 2009;125:2586–94.
33. Cambien B, Karimdjee BF, Richard-Fiardo P, Bziouech H, Barthel R, Millet MA, et al. Organ-specific inhibition of metastatic colon carcinoma by CXCR3 antagonism. Br J Cancer 2009;100:1755–64.
34. Picelli S, Bjorklund AK, Faridani OR, Sagasser S, Winberg G, Sandberg R. Smart-seq2 for sensitive full-length transcriptome profiling in single cells. Nat Methods 2013;10:1096–8.
35. Sui T, Wang X, Li L, Liu J, Qiao N, Duan L, et al. GOLM1 suppresses autophagy-mediated anti-tumor immunity in hepatocellular carcinoma. Signal Transduct Target Ther 2021;6:335.
36. Jain S, Jirau-Serrano X, Zullo KM, Scotto L, Palermo CF, Sastra SA, et al. Preclinical pharmacologic evaluation of pralatrexate and romidepsin confirms potent synergy of the combination in a murine model of human T-cell lymphoma. Clin Cancer Res 2015;21:2096–106.
37. Guan XW, Wang HQ, Ban WW, Chang Z, Chen HZ, Jia L, et al. Novel HDAC inhibitor chidamide synergizes with rituximab to inhibit diffuse large B-cell lymphoma tumour growth by upregulating CD20. Cell Death Dis 2020;11:20.
38. Limagne E, Nuttin L, Thibaudin M, Jacquin E, Aucagne R, Bon M, et al. MEK inhibition overcomes chemoimmunotherapy resistance by inducing CXCL10 in cancer cells. Cancer Cell 2022;40:136–52.
39. Karin N. Chemokines and cancer: new immune checkpoints for cancer therapy. Curr Opin Immunol 2018;51:140–5.
40. Chow MT, Ozga AJ, Servis RL, Frederick DT, Lo JA, Fisher DE, et al. Intratumoral activity of the CXCR3 chemokine system is required for the efficacy of anti-PD-1 therapy. Immunity 2019;50:1498–512.
41. Yan Y, Zheng L, Du Q, Yazdani H, Dong K, Guo Y, et al. Interferon regulatory factor 1(IRF-1) activates anti-tumor immunity via CXCL10/CXCR3 axis in hepatocellular carcinoma (HCC). Cancer Lett 2021;506:95–106.
42. Karagianni P, Wong J. HDAC3: taking the SMRT-N-CoRrect road to repression. Oncogene 2007;26:5439–49.
43. Wu SE, Hashimoto-Hill S, Woo V, Eshleman EM, Whitt J, Engleman L, et al. Microbiota-derived metabolite promotes HDAC3 activity in the gut. Nature 2020;586:108–12.
44. Tong L, Liang H, Zhuang H, Liu C, Zhang Z. The relationship between HDAC3 and malignant tumors: a mini review. Crit Rev Eukaryot Gene Expr 2020;30:279–84.
45. Zhang L, Chen Y, Jiang Q, Song W, Zhang L. Therapeutic potential of selective histone deacetylase 3 inhibition. Eur J Med Chem 2019;162:534–42.
46. Nguyen HCB, Adlanmerini M, Hauck AK, Lazar MA. Dichotomous engagement of HDAC3 activity governs inflammatory responses. Nature 2020;584:286–90.
47. Sun Z, Miller RA, Patel RT, Chen J, Dhir R, Wang H, et al. Hepatic Hdac3 promotes gluconeogenesis by repressing lipid synthesis and sequestration. Nat Med 2012;18:934–42.
48. Knutson SK, Chyla BJ, Amann JM, Bhaskara S, Huppert SS, Hiebert SW. Liver-specific deletion of histone deacetylase 3 disrupts metabolic transcriptional networks. EMBO J 2008;27:1017–28.
49. Sun Z, Feng D, Fang B, Mullican SE, You SH, Lim HW, et al. Deacetylase-independent function of HDAC3 in transcription and metabolism requires nuclear receptor corepressor. Mol Cell 2013;52:769–82.
50. Zhang L, Cai M, Gong Z, Zhang B, Li Y, Guan L, et al. Geminin facilitates FoxO3 deacetylation to promote breast cancer cell metastasis. J Clin Invest 2017;127:2159–75.